J|A|C|S
ARTICLES
Published on Web 11/28/2002

Elucidation of a Low Spin Cobalt(II) System in a Distorted Tetrahedral Geometry

David M. Jenkins, Angel J. Di Bilio, Matthew J. Allen, Theodore A. Betley, and Jonas C. Peters*

Contribution from the Division of Chemistry and Chemical Engineering, Arnold and Mabel Beckman Laboratories of Chemical Synthesis, California Institute of Technology, Pasadena, California 91125

Received April 5, 2002. Revised Manuscript Received September 27, 2002

Abstract: We have prepared a series of divalent cobalt(II) complexes supported by the [$PhBP_3$] ligand ([$PhBP_3$] = [$PhB(CH_2PPh_2)_3]^-$) to probe certain structural and electronic phenomena that arise from this strong field, anionic tris(phosphine) donor ligand. The solid-state structure of the complex [$PhBP_3$]CoI (**1**), accompanied by SQUID, EPR, and optical data, indicates that it is a pseudotetrahedral cobalt(II) species with a doublet ground state—the first of its type. To our knowledge, all previous examples of 4-coordinate cobalt(II) complexes with doublet ground states have adopted square planar structure types. Complex **1** provided a useful precursor to the corresponding bromide and chloride complexes, $\{[PhBP_3]Co(\mu\text{-Br})\}_2$, (**2**), and $\{[PhBP_3]Co(\mu\text{-Cl})\}_2$, (**3**). These complexes were similarly characterized and shown to be dimeric in the solid-state. In solution, however, the monomeric low spin form of **2** and **3** dominates at 25 °C. There is spectroscopic evidence for a temperature-dependent monomer/dimer equilibrium in solution for complex **3**. Furthermore, the dimers **2** and **3** did not display appreciable antiferromagnetic coupling that is typical of halide and oxo-bridged copper(II) and cobalt(II) dimers. Rather, the EPR and SQUID data for solid samples of **2** and **3** suggest that they have triplet ground states. Complexes **1**, **2**, and **3** are extremely oxygen sensitive. Thus, stoichiometric oxidation of **1** by dioxygen produced the 4-coordinate, high spin complex $[PhB(CH_2P(O)Ph_2)_2(CH_2PPh_2)]$CoI, (**4**), in which the [$PhBP_3$] ligand had undergone a 4-electron oxidation. Reaction of **1** with TlOAr (Ar = 2,6-Me_2Ph) afforded an example of a 4-coordinate, high spin complex, [$PhBP_3$]Co(O-2,6-Me_2Ph) (**5**), with an intact [$PhBP_3$] ligand. The latter two complexes were spectroscopically and structurally characterized for comparison to complexes **1**, **2**, and **3**. Our data for these complexes collectively suggest that the [$PhBP_3$] ligand provides an unusually strong ligand-field to these divalent cobalt complexes that is chemically distinct from typical tris(phosphine) donor ligand sets, and distinct from tridentate borato ligands that have been previously studied. Coupling this strong ligand-field with a pronounced axial distortion away from tetrahedral symmetry, a geometric consequence that is enforced by the [$PhBP_3$] ligand, provides access to monomeric [$PhBP_3$]CoX complexes with doublet rather than quartet ground states.

I. Introduction

Metal centers that reside in unusual coordination geometries sometimes display unique physical properties that correlate to novel modes of chemical reactivity. Metalloenzymes can exploit subtle structure/function relationships to achieve specific catalytic transformations by intimately tuning the local stereochemistry and ligand-field in a protein active site.[1] An appreciation of specific ligand-to-metal interactions in protein active sites is therefore highly dependent on our basic understanding of elementary stereochemical and ligand-field relationships in coordination chemistry.[2−5] Moreover, our community's general desire to make use of these elementary principles to rationally design catalysts selective for specific transformations motivates ongoing interest in this area.[6,7] In this paper, we suggest that coupling (i) an axial distortion in a pseudo-tetrahedral cobalt(II) complex of approximate 3-fold symmetry with (ii) a strong ligand-field donor strength can provide access to a doublet rather than a quartet electronic ground state. This result is of interest because, to the best of our knowledge, all previously characterized 4-coordinate cobalt(II) systems that are low-spin have adopted approximate square planar structure types.[8,9] Owing to its historically well-behaved and rich spectroscopy, there has

(1) Lippard, S. J.; Berg, J. M. *Principles of Bioinorganic Chemistry*; University Science Books: Mill Valley, CA, 1994; Chapter 12.
(2) (a) Halpern, J. *Science* **1985**, *227*, 869−875. (b) Geno, M. K.; Halpern, J. *J. Am. Chem. Soc.* **1987**, *109*, 1238−1240.
(3) Perutz, M. F.; Fermi, G.; Luisi, B.; Shaanan, B.; Liddington, R. C. *Acc. Chem. Res.* **1987**, *20*, 309−321.
(4) Raphael, A. L.; Gray, H. B. *J. Am. Chem. Soc.* **1991**, *113*, 1038−1040.
(5) Garret, T. P. J.; Glingeleffer, D. J.; Guss, J. M.; Rogers, S. J.; Freeman, H. C. *J. Biol. Chem.* **1984**, *259*, 2822−2825.
(6) Schultz, B. E.; Gheller, S. F.; Muetterties, M. C.; Scott, M. J.; Holm, R. H. *Acc. Chem. Res.* **1986**, *19*, 363−370.
(7) Sellmann, D.; Sutter, J. *Acc. Chem. Res.* **1997**, *30*, 460−469.
(8) (a) Everett, G. W.; Holm, R. H. *J. Am. Chem. Soc.* **1965**, *87*, 5266−5267. (b) Cotton, F. A.; Soderberg, R. H. *J. Am. Chem. Soc.* **1962**, *84*, 872−873. Also see the general references 21, 22, and 38.
(9) Stereochemical tuning of 4-coordinate structure types of cobalt(II), and the ground spin-state consequences of such tuning, has been recently described: Jaynes, B. S.; Doerrer, L. H.; Liu, S.; Lippard, S. J. *Inorg. Chem.* **1995**, 34, 5735−5744.

10.1021/ja026433e CCC: $22.00

been longstanding interest in using cobalt(II) substitution to probe local stereochemical environments in the active sites of native enzymes. Perhaps the most familiar example of this use is that of zinc carbonic anhydrase.[10] Establishing that pseudo-tetrahedral cobalt(II) can exhibit spectroscopic features consistent with a doublet rather than a quartet ground state is particularly interesting in this latter context.

The series of paramagnetic cobalt complexes described below is well suited to probing the ligand-field donor strength that is imposed by the tris(phosphino)borate ligand $[PhB(CH_2PPh_2)_3]^-$, abbreviated throughout as $[PhBP_3]$.[11,12] The recently introduced $[PhBP_3]$ ligand[13] is a structurally similar but anionic relative to the well-known tris(phosphine) ligand $CH_3C(CH_2PPh_2)_3$ (abbreviated as triphos herein)[14−16] that was originally reported by Hewertson and Watson in 1964.[17] Our continued focus on developing neutral complexes that feature a partially insulated borate counteranion, fixed at a short but remote distance from a transition metal that is coordinated by neutral amine or phosphine donor arms, is in part due to the promise these formal zwitterions hold for catalytic applications.[18,19] Studying the elementary and catalytic reaction processes of zwitterions of this type, and comparing their reactivity to isostructural but more conventional cationic relatives, is paramount to defining the role zwitterionic systems might offer to homogeneous catalysis. It is also of interest to examine the impact that the fastened borate unit can have upon the intimate electronic structure of the coordinated metal center. This study describes our initial efforts to address this latter issue. We provide evidence to show that, when coordinated to a cobalt(II) ion, the $[PhBP_3]$ anion provides access to a unique low spin cobalt(II) complex, $[PhBP_3]CoI$ (**1**),

Scheme 1

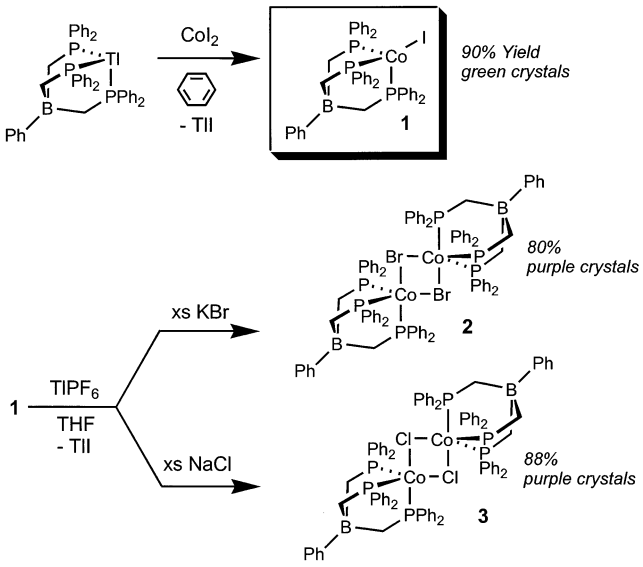

whose stereochemical structure is best regarded as distorted tetrahedral.[20] Given the intense spectroscopic and magnetic scrutiny divalent cobalt has received during the past several decades,[21,22] elucidation of this low spin system is particularly interesting. Complex **1** and its chloride and bromide relatives are structurally related to the well-known but cationic, triphos-supported cobalt(II) systems popularized by Sacconi and more recently by Huttner.[23,24] The data presented in this paper affords a first comparative glance at the dramatic electronic consequences that arise when the borate counteranion is embedded within the phosphine donor ligand framework.

The synthetic, structural, and spectroscopic data for the title complex **1** are presented below to corroborate its low spin assignment. Two related low spin cobalt(II) derivatives, $\{[PhBP_3]Co^{II}X\}$ (X = Br, Cl), are also described. These latter two complexes feature an added complexity in that they are dimeric in the solid-state, but predominantly monomeric in solution. The collection of comparative solid-state and solution EPR spectra for **1**, **2**, and **3** is presented. For comparison, structural and spectroscopic data for two high spin derivatives that were obtained directly from **1** are also described.

II. Results

IIa. Synthesis and Solid-State Structures of $\{[PhBP_3]Co^{II}X\}$ (X = I, Br, Cl). Scheme 1 presents the synthesis of the three halide derivatives $\{[PhBP_3]Co^{II}X\}$ (X = I, Br, Cl). The high yield synthesis of the iodide complex $[PhBP_3]CoI$, (**1**), derived from the thallium reagent $[PhBP_3]Tl$, has been previously described.[18c] Although the bromide and chloride derivatives could be similarly prepared, they were best derived

(10) (a) Solomon, E. I.; Rawlings, J.; McMillin, J. R.; Stephens, P. J.; Gray, H. B. *J. Am. Chem. Soc*. **1976**, *98*, 8046−8048. (b) Bertini, I.; Luchinat, C. *Acc. Chem. Res.* **1983**, *16*, 272−279. (c) Bertini, I.; Lanini, G.; Luchinat, C. *J. Am. Chem. Soc*. **1983**, *105*, 5116−5118. (d) Khalifah, R. G.; Rogers, J. I.; Harmon, P.; Morely, P. J.; Carroll, S. B. *Biochemistry* **1984**, *23*, 3129−3136. (e) Briganti, F.; Pierattelli, R.; Scozzafava, A.; Supuran, C. T. *Eur. J. Med. Chem*. **1996**, *31*, 1001−1010.

(11) Cobalt complexes supported by tris(pyrazolyl)borate ligands have been studied extensively. For recent examples, see: (a) Detrich, J.; Koneèny-Vetter, W. M.; Doren, D.; Rheingold, A. L.; Theopold, K. H. *J. Am. Chem. Soc*. **1996**, *118*, 1703−1712. (b) Jewson, J. D.; Liable-Sands, L. M.; Yap, G. P. A.; Rheingold, A. L.; Theopold, K. H. *Organometallics* **1999**, *18*, 300−305. (c) Thyagarajan, S.; Incarvito, C. D.; Rheingold, A. L.; Theopold, K. H. *Chem. Commun*. **2001**, 2198−2199.

(12) Cobalt complexes supported by tris(thioether)borate ligands have been studied recently. See: Schebler, P.; Mondimutsira, B.; Riordan, C. G.; Liable-Sands, L. M.; Incarvito, C. D.; Rheingold, A. L. *J. Am. Chem. Soc*. **2001**, *123*, 331−332.

(13) (a) Peters, J. C.; Feldman, J. D.; Tilley, T. D. *J. Am. Chem. Soc*. **1999**, *121*, 9871−9872. (b) Barney, A. A.; Heyduk, A. F.; Nocera, D. G. *Chem. Commun*. **1999**, 2379−2380.

(14) The abbreviation *triphos* is used herein to designate the tripodal, tridentate ligand $RC(CH_2PPh_2)_3$ (R = alkyl or aryl). This abbreviation is often used to delineate tridentate phosphines of the type $PhP(CH_2PPh_2)_2$. In this manuscript, we restrict our use of the term *triphos* to represent the former ligand class.

(15) (a) Benelli, C.; DiVaira, M.; Noccioli, G.; Sacconi, L. *Inorg. Chem*. **1977**, *16*, 182−187. (b) Ghilardi, C.; Midollina, S.; Orlandini, A.; Sacconi, L. *Inorg. Chem*. **1980**, *19*, 301−306. (c) Dapparto, P.; Midollini, S.; Orlandini, A.; Sacconi, L. *Inorg. Chem*. **1976**, *15*, 2768−2744.

(16) For recent papers dealing with (triphos)Co^{2+} chemistry, see: (a) Heinze, K.; Huttner, G.; Walter, O. *Eur. J. Inorg. Chem*. **1999**, 593−600. (b) Heinze, K.; Huttner, G.; Schober, P. *Eur. J. Inorg. Chem*. **1998**, 183−189. (c) Heinze, K.; Huttner, G.; Zsolnai, L. *Z. Naturforsch. (B)* **1999**, *54*, 1147−1154. (d) Winterhalter, U.; Zsolnai, L.; Kirscher, P.; Heinz, K.; Huttner, G. *Eur. J. Inorg. Chem*. **2001**, 89−103. (e) Rupp, R.; Huttner, G.; Kirscher, P.; Soltek, R.; Büchner, M. *Eur. J. Inorg. Chem*. **2000**, 1745−1757.

(17) Hewertson, W.; Watson, H. R. *J. Chem. Soc*. **1962**, 1490−1494.

(18) (a) Lu, C. C.; Peters, J. C. *J. Am. Chem. Soc*. **2002**, *124*, 5273−5273. (b) Thomas, J. C.; Peters, J. C. *J. Am. Chem. Soc*. **2001**, *123*, 5100−5101. (c) Shapiro, I. R.; Jenkins, D. M.; Thomas, J. C.; Day, M. W.; Peters, J. C. *Chem. Commun*. **2001**, 2152−2153. (d) Jenkins, D. M.; Betley, T. A.; Peters, J. C. *J. Am. Chem. Soc*. **2002**, *124*, 11238−11239.

(19) We have recently prepared the bis(amino)borate ligand $[Ph_2B(CH_2NMe_2)_2]^-$. Betley, T. A.; Peters, J. C. *Inorg. Chem*. **2002**, in press.

(20) This finding was briefly described in a previous communication. See ref 18c.

(21) For a lucid discussion of cobalt(II) EPR spectroscopy, see: Bencini, A.; Gatteschi, D. *Trans. Metal Chem*. **1982**, *8*, 97−119.

(22) A thorough discussion of the electronic structure of cobalt(II) systems in 4-, 5-, and 6-coordinate geometries has been provided by Lever: Lever, A. B. P. *Inorganic Electronic Spectroscopy*, 2nd ed.; Elsevier: New York, 1984; pp 480−505.

(23) (a) Sacconi, L.; Midollini, S. *J. Chem. Soc., Dalton. Trans*. **1972**, 1213−1216. (b) Dapporto, P.; Midollini, S.; Sacconi, L. *Inorg. Chem*. **1975**, *14*, 1643−1650. (c) Mealli, C.; Midollini, S.; Sacconi, L. *Inorg. Chem*. **1975**, *14*, 2513−2521. (d) Ghilardi, C. A.; Midollini, S.; Sacconi, L. *J. Organomet. Chem*. **1980**, *186*, 279−287.

(24) See Heinze, K.; Huttner, G.; Zsolnai, L.; Schober, P. *Inorg. Chem*. **1997**, *36*, 5457−5469.

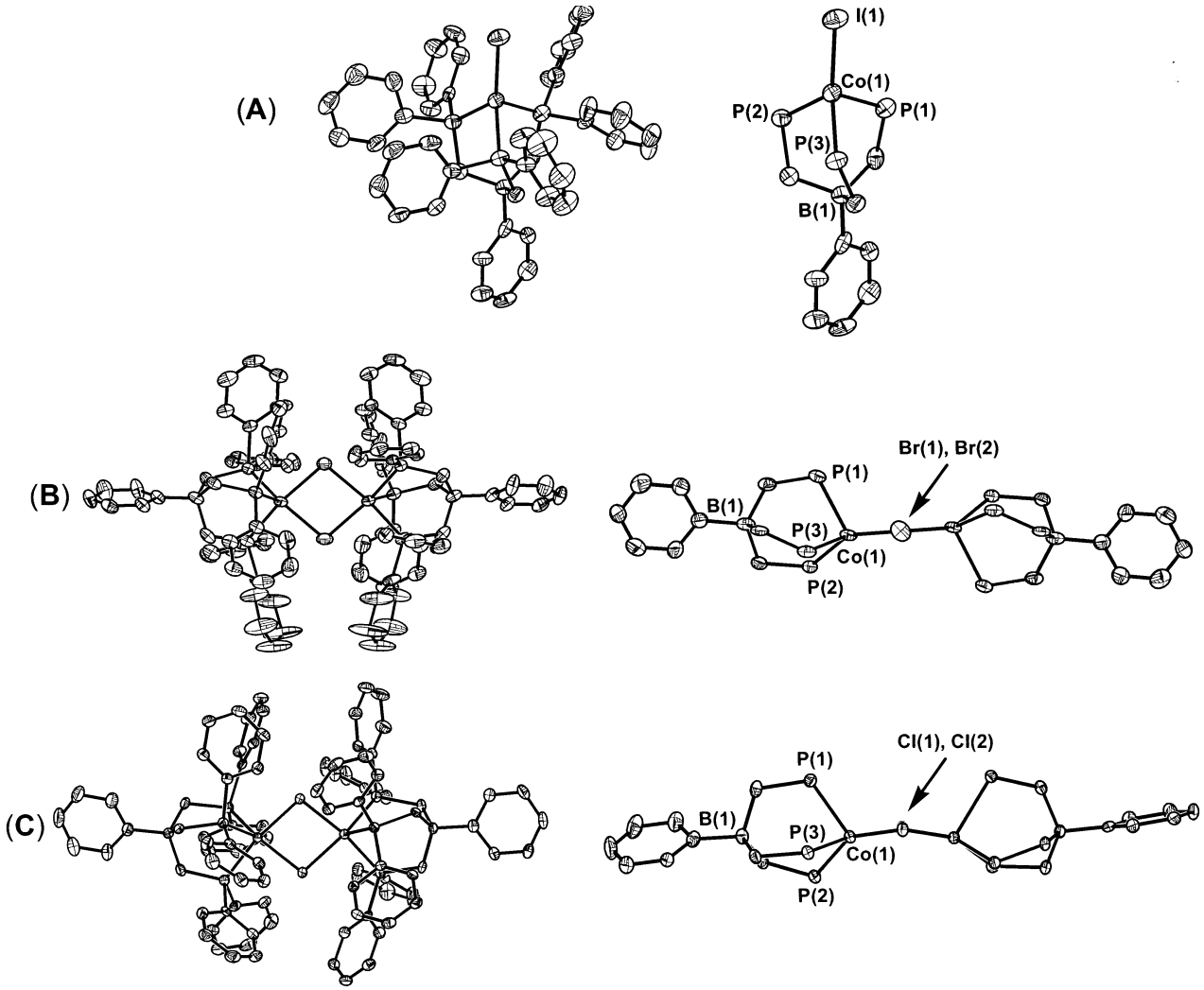

Figure 1. Displacement ellipsoids are represented at 50%. Structures on the right are shown without aryl carbon atoms for clarity and the dimers are rotated such that the bridging halide ligands are eclipsed. **(A) [PhBP$_3$]CoI, (1);** Selected interatomic distances (Å) and angles (deg) for each independent molecule in crystal structure: Co(1)−P(1), 2.200(2); Co(1)−P(2), 2.206(2); Co(1)−P(3), 2.282(2); Co(1)−I(1), 2.488(1); Co(1)−B(1), 3.490(8). P(1)−Co(1)−P(2), 90.33(8); P(1)−Co(1)−P(3), 94.46(7); P(2)−Co(1)−P(3), 91.95(7); P(1)−Co(1)−I(1), 117.54(6); P(2)−Co(1)−I(1), 129.19(6); P(3)−Co(1)−I(1), 124.01(6). **(B) {[PhBP$_3$]Co(μ-Br)}$_2$, (2);** Selected interatomic distances (Å) and angles (deg): Co(1)−Co(1)#1, 3.668(1); Co(1)−P(3), 2.235(2); Co(1)−P(2), 2.247(2); Co(1)−P(1), 2.336(2); Co(1)−Br(1), 2.413(1); Co(1)−Br(2), 2.424(1); Co(1)−B(1), 3.570(6). Co(1)−Br(1)−Co(1)#1, 98.97(5); Co(1)−Br(2)−Co(1)#1, 98.37(5); P(3)−Co(1)−P(2), 87.42(6); P(3)−Co(1)−P(1), 92.35(6); P(2)−Co(1)−P(1), 93.44(6); P(3)−Co(1)−Br(1), 165.70(5); P(2)−Co(1)−Br(1), 93.63(5); P(1)−Co(1)−Br(1), 101.81(4); P(3)−Co(1)−Br(2), 91.35(5); P(2)−Co(1)−Br(2), 153.37(5); P(1)−Co(1)−Br(2), 113.19(4); Br(1)−Co(1)−Br(2), 81.33(3). Symmetry transformations used to generate equivalent atoms: #1 $-x, y, -z + 1/2$. **(C) {[PhBP$_3$]Co(μ-Cl)}$_2$, (3);** Selected interatomic distances (Å) and angles (deg): Co(1)−Co(2), 3.497(1); Co(1)−B(1), 3.551(3); Co(2)−B(2), 3.598(3); Co(1)−P(1), 2.224(1); Co(1)−P(2), 2.244(1); Co(1)−P(3), 2.391(1); Co(1)−Cl(1), 2.284(1); Co(1)−Cl(2), 2.321(1); Co(2)−P(4), 2.227(1); Co(2)−P(5), 2.239(1); Co(2)−P(6), 2.336(1); Co(2)−Cl(1), 2.314(1); Co(2)−Cl(2), 2.332(1). Co(1)−Cl(1)−Co(2), 99.02(3); Co(1)−Cl(2)−Co(2), 97.46(3); P(1)−Co(1)−P(2), 88.16(3); P(1)−Co(1)−Cl(1), 162.76(3); P(2)−Co(1)−Cl(1), 92.82(3); P(1)−Co(1)−Cl(2), 92.55(3); P(2)−Co(1)−Cl(2), 159.70(3); Cl(1)−Co(1)−Cl(2), 80.65(2); P(1)−Co(1)−P(3), 91.09(3); P(2)−Co(1)−P(3), 92.66(3); Cl(1)−Co(1)−P(3), 106.04(3); Cl(2)−Co(1)−P(3), 107.60(3); Cl(1)−Co(2)−Cl(2), 79.79(2).

metathetically from the iodide complex: in situ iodide abstraction by $TlPF_6$ in THF, followed by addition of KBr or NaCl, converted [PhBP$_3$]CoI to {[PhBP$_3$]Co(μ-Br)}$_2$, (**2**), and {[PhBP$_3$]-Co(μ-Cl)}$_2$, (**3**), respectively. Complexes **2** and **3** were isolated in yields typically greater than 80% when the metathesis protocol was repeated twice prior to workup. The halide derivatives **1**, **2**, and **3** gave rise to distinct and well-resolved, though paramagnetically shifted, ^{1}H NMR spectra that are provided for reference in the Supporting Information.

The iodide complex **1** is green whereas the chloride and bromide complexes **2** and **3** are purple in the crystalline state. This difference in color between polycrystalline samples of the three complexes correlates with their solid-state structures, which were determined by low-temperature X-ray diffraction studies. Displacement ellipsoid representations for the solid-state structures (collected at 98 K) of **1**, **2**, and **3** are depicted in Figure 1A, 1B, and 1C, respectively. The structure shown to the right for each complex provides a simplified representation in which the aryl carbon atoms from the diphenylphosphine donors have been omitted. Furthermore, the structures on the right of the bromide and chloride derivatives are rotated so that the bridging halide ligands are eclipsed. Only the bridged halide protruding out of the plane of the page is visible.

Most striking in Figure 1 is the monomeric structure obtained for the iodide complex **1** in comparison to the dimeric solid-state structures obtained for the bromide and chloride complexes **2** and **3**, respectively. Although none of the three complexes adopts an idealized local geometry, they can be approximated

as structure types typical of cobalt(II). The iodide **1** is best described as pseudotetrahedrally coordinated, with low formal symmetry due to a strong axial distortion and inequivalent Co-phosphine bond lengths and angles. By contrast, the bromide and chloride derivatives can be regarded as square pyramidal structures at the localized cobalt center of each respective dimeric unit. In each of the three structures, the tridentate [$PhBP_3$] ligand exhibits two short and one modestly elongated Co−P bond. The P−Co−P angles vary only slightly from 90°.

The bromide complex **2** features a rigorously planar Co_2Br_2 rhombus that is bisected by a crystallographic C_2-axis running through the two bromide ligands. The C_2-axis effectively places the elongated axial Co−P bonds on opposite faces of the Co_2Br_2 plane. By comparison, the Co_2Cl_2 unit of the chloride complex **3** gently buckles from planarity. The two elongated, axial Co−P bonds in this case reside on the same face of the Co_2Cl_2 unit. The gentle buckling in **3**, along with the decreased size of the chloride bridge, effectively slides the two cobalt centers closer together by comparison to their distance in **2** (3.668(1) Å in **2** versus 3.497(1) Å in **3**). Dimeric **3** is structurally very similar to its dicationic relative [{(triphos)Co(μ-Cl)}$_2$][BPh_4]$_2$: the Co−Co distance in [{(triphos)Co(μ-Cl)}$_2$][BPh_4]$_2$ is 3.52 Å, and its Co−Cl−Co angle is 100.0°, to be compared with an average Co−Cl−Co angle of 98.2° in **3**.[23c,24] The solid-state structure of [{(triphos)Co(μ-OH)}$_2$][BPh_4]$_2$ has also been determined and is similarly dimeric, though the O−Co−O angles are much smaller and average 69.5°.[23c] Spectroscopic data confirms that the bromide derivative [{(triphos)Co(μ-Br)}$_2$][BPh_4]$_2$ is dimeric as well;[23c] its solid-state crystal structure has not yet been reported.

The solid-state structure of the iodide complex **1** exhibits approximate C_s symmetry.[25] An appreciable axial distortion gives rise to I−Co−P bond angles that are much larger than those found in idealized tetrahedral structures (P(1)−Co(1)−I(1), 117.54(6); P(2)−Co(1)−I(1), 129.19(6); P(3)−Co(1)−I(1), 124.01(6)). Complex **1** is gently distorted from molecular 3-fold symmetry by a modest elongation of one of its phosphine donors by comparison to the other two (Co(1)−P(1), 2.200(2); Co(1)−P(2), 2.206(2); Co(1)−P(3), 2.282(2)). Worth noting is that monomeric **1** is formally a 15 electron complex; this is very unusual for cobalt(II) systems supported by three phosphine donors. Similar 15 electron, monomeric and pseudotetrahedral cobalt(II) halides supported by tris(pyrazolyl)- and tris(thioether)borate ligands have been reported previously.[26,27] An attempted synthesis of the analogous "[(triphos)CoI]$^+$" system was reported to have failed due to spontaneous reduction of the cobalt(II) center to cobalt(I).[23c]

IIb. Magnetic Data (SQUID) for {[PhBP$_3$]Co^{II}X} (X = I, Br, Cl). The temperature dependence of the magnetic susceptibility for complexes **1**, **2**, and **3** was studied by SQUID magnetometry. Average magnetic moments were adjusted for diamagnetic contributions using Pascal's constants and were fitted in the temperature range specified to use data that obeyed the Curie−Weiss law reasonably well. This was established from χ_m^{-1} versus T plots, which are shown in Figures 2b and 3b. For each case, the samples studied by SQUID magnetometry had provided satisfactory combustion analyses, as recorded in the Experimental Section. These same sample batches were also used to obtain the EPR spectra that are discussed in the following section.

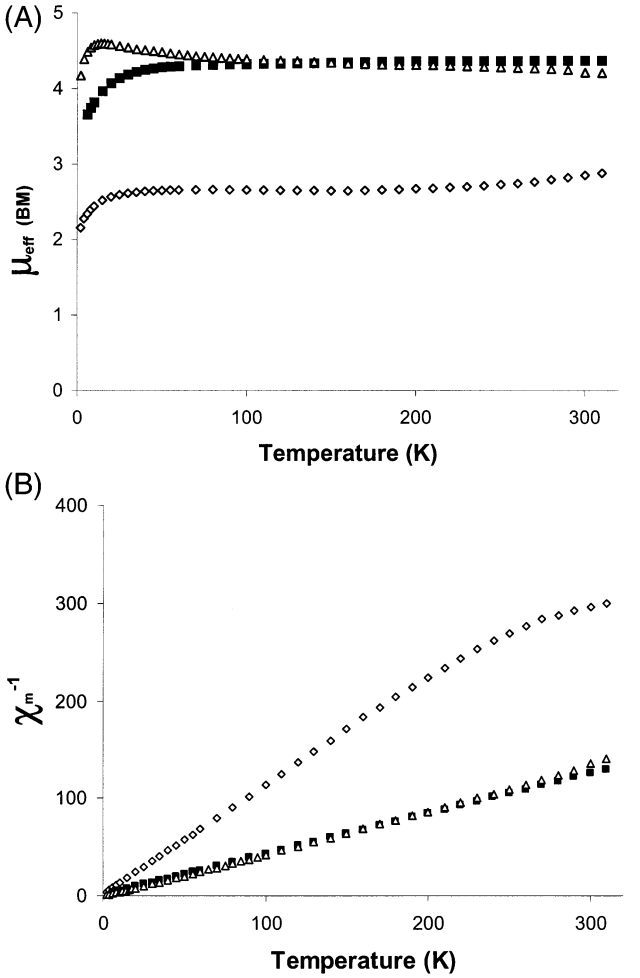

Figure 2. (A) SQUID plot of μ_{eff} (BM) versus T: [$PhBP_3$]CoI, **1**, (◇); [$PhB(CH_2PPh_2)(CH_2P(O)Ph_2)_2$]CoI, **4**, (■); [$PhBP_3$]Co(O-2,6-dimethylphenyl), **5**, (△). (B) SQUID plot of χ_m^{-1} (mol/cm^3) versus T: [$PhBP_3$]CoI, **1**, (◇); [$PhB(CH_2PPh_2)(CH_2P(O)Ph_2)_2$]CoI, **4**, (■); [$PhBP_3$]Co(O-2,6-dimethylphenyl), **5**, (△).

Figure 2a displays the temperature dependence of the calculated magnetic moment μ_{eff} (see Experimental Section for details) for complex **1**, and Figure 2b plots its χ_m^{-1} versus temperature. A χ_m versus temperature plot for **1** is provided in the Supporting Information. The magnetic data for **1** is unexpected for a 4-coordinate cobalt(II) system in a pseudotetrahedral coordination geometry. Its magnetic moment shows little variation in the temperature range between 30 and 220 K. The Curie law observed in this range indicates that the doublet state is the only state that is thermally populated. At very low temperature, intermolecular exchange phenomena likely quench the bulk paramagnetism ($\Theta = -1.38 \pm 1.27$ K). Above 220 K, the effective moment increases, albeit very gradually, possibly suggesting that a high spin state is slightly but increasingly populated as the temperature rises above 220 K. The concentration of a high spin state at the elevated temper-

(25) Complex **1** contained two crystallographically independent molecules in the asymmetric unit. For brevity, only one of the molecules is explicitly discussed in the main text. The Supporting Information contains crystal coordinates, bond lengths, and bond angles for both molecules of the asymmetric unit.

(26) Reinaud, O.; Rheingold, A.; Theopold, K. *Inorg. Chem.* **1994**, *33*, 2306−2308.

(27) For a discussion of high spin [PhTt$^{tert\text{-}butyl}$]CoCl see: Schebler, P.; Riordan, C.; Guzei, I.; Rheingold, A. *Inorg. Chem.* **1998**, *37*, 4754−4755. The complex [PhTt$^{tert\text{-}butyl}$]CoI has also been fully characterized but is not yet published (Riordan, C., personal communication).

atures is very small, however, as even at 300 K the value for μ_{eff} only reaches 2.85 μ_B. We note that the gradual rise in the moment that is observed above 220 K for **1** was reproducible and does not appear to be an artifact of the experiment. An average magnetic moment of 2.67 μ_B was obtained for **1** by fitting the susceptibility data in the temperature range between 10 and 310 K. A fit to the region from 30 to 220 K, where the sample shows good Curie−Weiss behavior, provides an average moment of 2.65 ± 0.03 μ_B, the error representing two standard deviations. For a 4-coordinate cobalt(II) complex, this moment would typically imply a cobalt(II) ion in an approximate *square planar* geometry.[28] Similar low spin moments are also common for cobalt(II) systems with higher coordination numbers (e.g., square pyramidal, trigonal bipyramidal, or octahedral type structures),[38] the value of 2.65 μ_B tending toward the high side of what has been typically observed for low spin cobalt(II). By contrast, magnetic moments for tetrahedral and pseudo-tetrahedral structure types more closely related to [PhBP$_3$]CoI (T_d, C_{3v}, and lower symmetries) typically fall within a range between 4.3 and 5.2 μ_B and are assigned as high spin.[38,42] The average g value of 3.06 that is extracted from the SQUID magnetization data, assuming a moment of 2.65 μ_B, is much higher than the effective g value directly obtained by solid-state EPR spectroscopy ($g \approx 2.1$), as discussed below. The crude relationship between g and μ_{eff}, as defined by the simplified equation $\mu_{eff} = g\{S(S+1)\}^{1/2}$, assumes complete quenching of an orbital contribution,[45] which may be a serious over-simplification in the present context. The room-temperature benzene solution magnetic moment of **1** was estimated by the method of Evans and provided a value of 2.87 μ_B, assuming a diamagnetic correction from Pascal's constants, in close agreement with that obtained from the SQUID data at 300 K.[29] We suggest that the solid-state and solution moments are most consistent with a low spin assignment for **1**, and that a low spin ground state is very reasonable for a complex of this type based upon the rationale provided in the discussion section. Moreover, the low spin assignment is further corroborated by the EPR data for **1**.

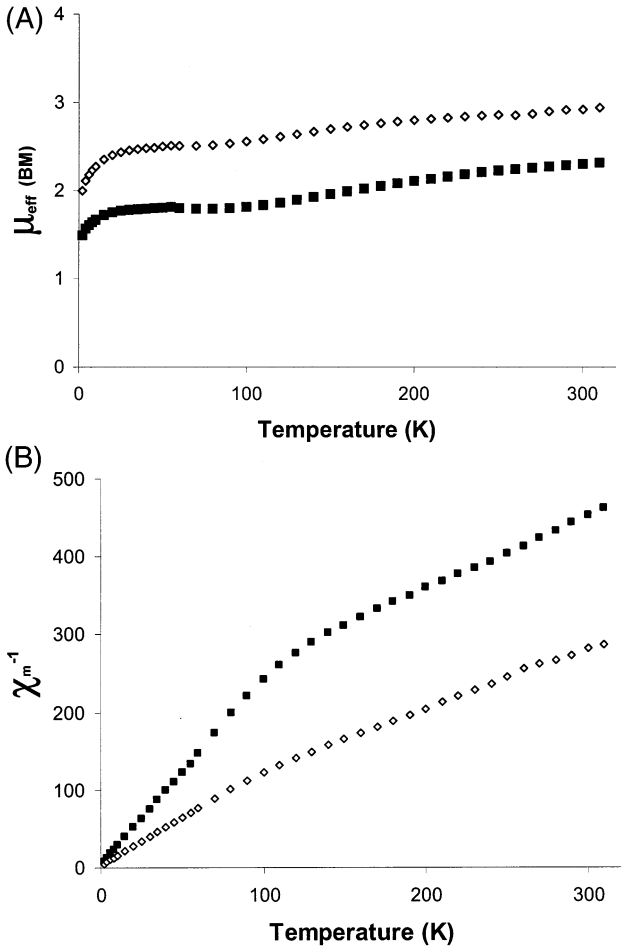

Figure 3. (A) SQUID plot of μ_{eff} (BM) versus T: {[PhBP$_3$]Co(μ-Br)}$_2$, **2**, (■);{[PhBP$_3$]Co(μ-Cl)}$_2$, **3**, (◇). (B) SQUID plot of χ_m^{-1} (mol/cm^3) versus T: {[PhBP$_3$]Co(μ-Br)}$_2$, **2**, (■);{[PhBP$_3$]Co(μ-Cl)}$_2$, **3**, (◇).

The solid-state magnetic susceptibilities for polycrystalline samples of the dimeric bromide {[PhBP$_3$]Co(μ-Br)}$_2$ and chloride {[PhBP$_3$]Co(μ-Cl)}$_2$ were also measured by SQUID magnetometry and are plotted, *per dimeric unit*, in Figure 3, parts A and B. The magnetic data obtained for the dimers is more complex than the data obtained for monomeric **1**. Each set of susceptibility data was collected twice to verify its experimental reproducibility. Little, if any, evidence for detectable antiferromagnetic coupling in dimers **2** and **3** can be gleaned from the temperature-dependent plots of μ_{eff} and χ_m^{-1}. The acid test for antiferromagnetic exchange coupling in a dimeric complex consisting of two spin $^1/_2$ ions is that the susceptibility should reach a maximum as the temperature of the sample is lowered, but then fall precipitously to zero as the sample is cooled further.[45] For both **2** and **3**, the magnetic moments decrease very gently from 310 K down to about 80 K, at which point they level off until reaching the lowest

(28) Casey, A. T.; Mitra, S. *Theory and Application of Molecular Paramagnetism*; Bourduaux, E. A., Mulay, N. L., Eds.; Wiley: New York, 1976.
(29) (a) Sur, S. K. *J. Magn. Reson*. **1989**, *82*, 169−173. (b) Evans, D. F. *J. Chem. Soc*. **1959**, 2003−2005.
(30) (a) Sinn, E. *Coord. Chem. Rev*. **1970**, *5*, 313−347, and references therein. (b) Ball, P. W. *Coord. Chem. Rev*. **1969**, *4*, 361−383. (c) Kato, M.; Jonassen, H. B.; Fanning, J. C. *Chem. Rev*. **1964**, *64*, 99−128.
(31) Ghilardi, C. A.; Mealli, C.; Midollini, S.; Nefedov, V. I.; Orlandini, A.; Sacconi, L. *Inorg. Chem*. **1980**, *19*, 2454−2462.
(32) Note that the solution susceptibilities for **2** and **3** are calculated by the Evans method assuming a *monomeric* formulation for each complex.
(33) Sealy, R.; Hyde, J. S.; Antholine, W. E. *Modern Physical Methods in Biochemistry*; Neuberger, A., Van Deenen, L. L. M., Eds.; Elsevier: New York, 1985; p 69.
(34) Superhyperfine coupling to phosphorous in a 5-coordinate cobalt(II) phosphine complex has been treated previously. See: Stelzer, O.; Sheldrick, W. S.; Subramanian, J. *J. Chem. Soc., Dalton Trans*. **1976**, 966−970.
(35) Gatteschi, D. *J. Mol. Catal*. **1985**, *23*, 145−150.
(36) Oxygenation of related (triphos)Co^{2+} complexes did *not* produce a similarly isolable species. See: Heinze, K.; Huttner, G.; Zsolnai, L. *Chem. Ber*. **1997**, *130*, 1393−1403.
(37) Banci, L.; Bencini, A.; Benelli, C.; Gatteschi, D.; Zanchini, C. *Struct. Bonding* **1982**, *52*, 37−86.
(38) Cotton, F. A.; Wilkinson, G. *Advanced Inorganic Chemistry*, 5th ed.; Wiley: New York, 1988; p 729. See ref 22 for a more thorough discussion and representative references.
(39) Osmometric measurements to determine the solution molecular weights of **2** and **3** by the method of Signer were vitiated due to the tendency of these species to precipitate from toluene and benzene solution at moderate concentrations.
(40) Sacconi, L.; Ciampolini, M.; Speroni, C. P. *Inorg. Chem*. **1965**, *4*, 1116−1119.
(41) Nicolini, M.; Pecile, C.; Turco, A. *J. Am. Chem. Soc*. **1965**, *87*, 2379−2384.
(42) For relevant references that deal with 4-coordinate cobalt(II) in approximate C_3 or C_{3v} symmetry, see the following: (a) Garrett, B. B.; Goedken, V. L.; Quagliano, J. V. *J. Am. Chem. Soc*. **1970**, *92*, 489−493. (b) Bertini, I.; Gatteschi, D.; Mani, F. *Inorg. Chim. Acta* **1973**, *7*, 717−720. (c) Gerloch, M.; Hanton, L. R. *Inorg. Chem*. **1980**, *19*, 1692−1698. (d) Gerloch, M.; Manning, M. R. *Inorg. Chem*. **1981**, *20*, 1051−1056. (e) Banci, L.; Benelli, C.; Gatteschi, D.; Mani, F. *Inorg. Chem*. **1982**, *21*, 1133−1136.
(43) A series of related 5-coordinate [PhBP$_3$]Co(II) complexes has been prepared that will be reported in due course.
(44) Jazdzewski, B. A.; Holland, P. L.; Pink, M.; Young, V. G.; Spencer, D. J. E.; Tolman, W. B. *Inorg. Chem*. **2001**, *40*, 6097−6107.
(45) Kahn, O. *Molecular Magnetism*; VCH Publishers: New York, 1993; pp 1−10.

temperature region where intermolecular paramagnetic quenching begins to occur. The expected maximum in the susceptibility for **2** and **3** is not observed, in contrast to the temperature-dependent susceptibilities Sacconi reported for [{(triphos)Co-(μ-X)}$_2$][BPh$_4$]$_2$ (X = Br, Cl, OH), indicating the dicationic dimers exhibit strong antiferromagnetic coupling ($J < -100$ cm^{-1}) between their Co^{2+} centers.[23c] Antiferromagnetic exchange behavior is most typical of halide-bridged cobalt(II), copper(II), and titanium(I) dimers, where an unpaired electron resides at each metal center,[30] and it is emphasized that antiferromagnetic exchange does not appear to be present in either **2** or **3**. The net change in the moment for both **2** and **3** is rather small between 300 and 80 K. For example, at 300 K the moment of chloride **3** is 2.9 μ_B, which decreases to 2.5 μ_B at 80 K. For bromide **2**, the moment at 300 K (2.3 μ_B) is appreciably lower than for **3** and only decreases to a value of 1.8 μ_B at 80 K. For a simple ferromagnetic exchange interaction ($J > 0$) between the two spin $^1/_2$ ions in dimers **2** and **3**, a plot of $\chi_m T$ versus T is expected to show a rise in the curve as the temperature is lowered. Instead, we observe a gentle decrease in $\chi_m T$ (and likewise μ_{eff}) as the temperature is lowered, which decreases dramatically only at very low temperature due to the onset of intermolecular magnetic quenching interactions. The $\chi_m T$ versus T plots can be found in the Supporting Information for **2** and **3**. A fit of the lower temperature data, where the Curie−Weiss law is obeyed reasonably well ($T < 110$ K), provided a magnetic moment $\mu_{eff} = 1.77 \pm 0.08$ μ_B and $\Theta = -1.48 \pm 0.49$ K for complex **2**. A moment of $\mu_{eff} = 2.47 \pm 0.14$ μ_B and theta value of $\Theta = -3.13 \pm 0.67$ K was obtained for complex **3** when fit in the same temperature regime. Zero-field splitting, weak exchange, and mixing of the triplet and singlet states of **2** and **3** likely complicate the observed magnetism and contribute to the gradual attenuation rather than rise of the moment of each sample as the temperature is lowered, as would have been expected for systems exhibiting pronounced ferromagnetic exchange. Regardless, we suggest that the magnetic data for **2** and **3** are most consistent with assigning them to $S = 1$ ground states. The EPR data for solid samples of **2** and **3** are also most consistent with a triplet ground state assignment (see below); the signal amplitude for these dimers increases as the temperature of each sample is lowered from 25 to 3.6 K, as is to be expected for a weak ferromagnetically coupled dimer with two $S = ^1/_2$ spin centers.

A dimeric cobalt(II) complex whose magnetism may be related to that observed for **2** and **3** was provided by Sacconi and co-workers in 1980.[31] They reported that the μ-thiolato complex, [{(triphos)Co(μ-SCH$_3$)}$_2$][BPh$_4$]$_2$, provided a μ_{eff} of 1.8 μ_B that gradually decreased to 0.8 μ_B at 130 K, at which point it leveled off down to the lowest temperature for which data was recorded (87 K). The reasoning Sacconi and co-workers provided to explain the odd magnetic behavior of [{(triphos)Co(μ-SCH$_3$)}$_2$][BPh$_4$]$_2$ was that antiferromagnetic exchange occurred between the spin $^1/_2$ cobalt centers through the μ-SCH$_3$ units, but that the limiting value represented a contribution from partial occupation of a higher triplet state. In our case, the limiting value at lower temperature represents a triplet state likely mixed with a singlet state that is close in energy.

It should be noted that the difference between the total μ_{eff} for solid samples of **2** and **3**, a difference of ca. 0.6 μ_B at 300 K, is not so pronounced in solution. Evans method measurements for **2** and **3** in benzene-d_6 at 25 °C provided moments of 2.7 μ_B and 3.0 μ_B, respectively, rather similar to the solution moment obtained for **1**.[32] As will be suggested by the EPR data discussed in the following section, these solution moments reflect a change in both geometry and spin state for **2** and **3** in toluene solution.

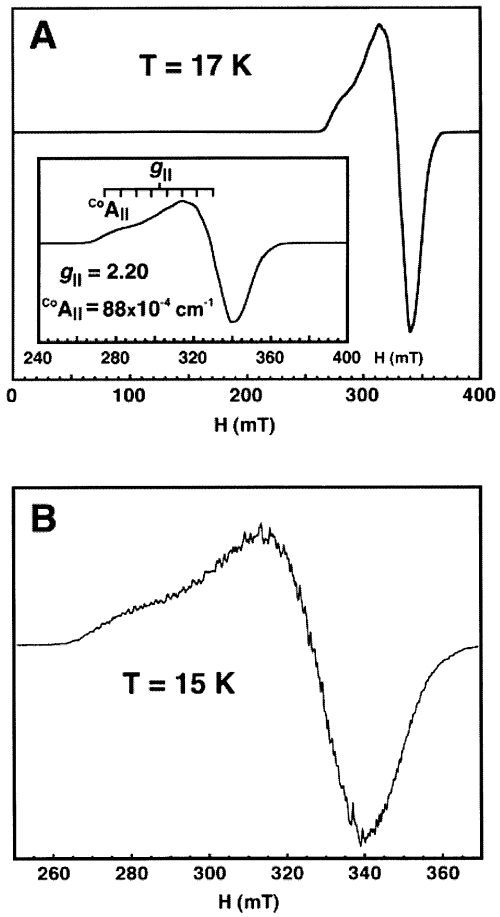

Figure 4. (A) EPR spectrum of a glassy toluene solution of [PhBP$_3$]CoI at 17 K. Instrumental parameters: $\nu = 9.477$ GHz, modulation frequency = 100 kHz, modulation amplitude = 4 G, microwave power = 0.51 mW, conversion time = 81.92 ms, time constant = 20.48 ms, 3 scans. $g \approx 2$ region and spectral assignment; $g_{||}$ and $A_{||}$ were estimated by simulating the EPR spectrum (inset). (B) EPR spectrum of a glassy toluene solution of [PhBP$_3$]CoI in toluene-d_8 at 15 K. Instrumental parameters: $\nu = 9.476$ GHz, modulation frequency = 100 kHz, modulation amplitude = 3 G, microwave power = 0.202 mW, conversion time = 81.92 ms, time constant = 20.48 ms, sweep time = 83.9 s, 3 scans.

IIc. EPR Spectra for {[PhBP$_3$]Co^{II}X} (X = I, Br, Cl). The EPR spectra for **1**, **2**, and **3** are extremely sensitive to oxygen due to a high spin impurity that results from a well-defined ligand oxidation process that has been carefully studied for the case of **1**. High-quality spectra for all three complexes were only acquired using thoroughly recrystallized samples that afforded satisfactory combustion analysis. The absence of high spin oxidation products was further confirmed by optical spectroscopy prior to EPR data collection.

The EPR spectrum in glassy toluene (17 K) of a pure sample of **1** is shown in Figure 4A. Due to the high oxygen sensitivity of **1**, the spectra that were originally obtained showed a rather broad feature in the region $g \approx 4.8$ (ca. 120 mT). This feature was entirely removed upon rigorous exclusion of oxygen from the sample. The broad feature at ~4.8 corresponds to a signal

Scheme 2

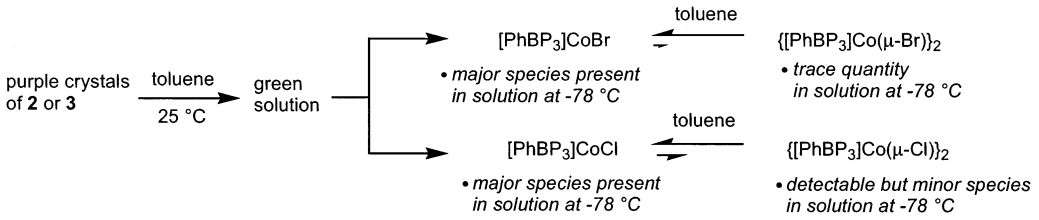

from the high spin complex **4**, whose independent characterization will be discussed shortly. The spectrum of pure **1** is nearly independent of temperature (except for its intensity) in the temperature range 20 K to 140 K. It is characterized by an axial g factor ($g_{||} = 2.20$ and $g_{\perp} = 2.05$), and poorly resolved ^{59}Co ($I = 7/2$) hyperfine splitting. However, a very complex superhyperfine splitting pattern was resolved below 50 K in toluene-d_8 (Figure 4B),[33] ascribable to the ^{31}P ($I = 1/2$)[34] and possibly ^{127}I$^-$ ($I = 5/2$) donor atoms. An isotropic EPR spectrum with $g_{iso} = 2.1$ was observable at room temperature, further confirming the low spin nature of **1**. The powder EPR spectrum of **1** shows features analogous to those of the frozen toluene sample, and a representative solid-state spectrum is provided in the Supporting Information. EPR signals for high spin cobalt(II) systems are typically observed only below ~30 K due to the fast spin−lattice relaxation times of the high spin Co(II) nucleus.[48] That we are able to observe an intense signal for **1** even at room-temperature further supports the notion that **1** has a doublet ground-state both in solution and in the solid-state.

The solid-state magnetic data that were presented above for **2** and **3** suggested that they each have triplet ground states close in energy to possibly mixed singlet excited states, and that the magnitude of exchange energy J is difficult to measure from the SQUID data alone. To the extent that ferromagnetic exchange is present, it is likely very small (<10 cm^{-1}). To further explore each of these systems, their EPR spectra were recorded using the same samples that had been carefully purified for the magnetic measurements. As for **1**, admission of adventitious oxygen to samples of **2** and **3** produced oxidation products (vide infra) that afforded spectra with signals centered at $g \approx 4.8$. Problematic is that these features coincidentally overlap with the low field EPR signal expected (and observed in the solid-state) for the pure dimers of **2** and **3**. Again, rigorous exclusion of oxygen solved this problem and high quality spectra were obtained. The EPR spectra (Figure 5A, 6A) for pure polycrystalline samples of both **2** and **3** are well resolved below 30 K. Each spectrum supports the suggestion of the triplet species at low temperature: the intensity of these spectra were not attenuated, but rather increased, from 25 to 3.6 K, consistent with weak ferromagnetic coupling. The temperature dependence of the solid-state EPR spectrum of **2** is shown in Figure 5d. We attempted to simulate the EPR spectra of the polycrystalline samples of **2** and **3** under the assumption that the exchange energy $|J| \gg$ than the X-band microwave quantum (0.3 cm^{-1}). In such cases the triplet state can be described in terms of D and E using the standard spin-Hamiltonian for an $S = 1$ spin system (see the Experimental Section).[48] We also made the crude assumption that the dipolar and g tensors were collinear.[35] Using this model, we could achieve only qualitative agreement between the simulated and experimental spectra. On the basis of these simulations, a zero-field splitting of roughly 0.2 cm^{-1} or less is consistent with the observed EPR spectra. Also, we note that the EPR spectrum of a monomeric triplet complex, [PhBP$_3$]Co(PMe$_3$), has been recorded and contains features qualitatively similar to those of **2** and **3** in the solid-state, including the low field g signal ~4.8. This system has been briefly described elsewhere.[18d]

Dissolution of *purple* crystals of {[PhBP$_3$]Co(μ-Br)}$_2$ (**2**) and {[PhBP$_3$]Co(μ-Cl)}$_2$ (**3**) in toluene was accompanied by a drastic color change to bright green, similar to the color of [PhBP$_3$]CoI both in solution and in the crystalline state. This behavior suggested to us a structural change in the dimers **2** and **3** upon dissolution. Indeed, we found by EPR that in solution a temperature-dependent equilibrium between monomeric and dimeric species seems to exist (Scheme 2). The EPR spectrum of **2** in glassy toluene (15 K) is shown in Figure 5b. This spectrum presumably represents a monomeric species akin to the structurally characterized iodide monomer, perhaps with an additional trace presence of the dimeric form of **2**. The observation that $g_{||} > g_{\perp}$ for **2** in the frozen glass clearly establishes that the square-pyramidal arrangement of the cobalt complex, observed in the solid-state, is not preserved in solution.[21] We suggest that the geometry of **2** in solution is that of a pseudotetrahedral, 4-coordinate monomer, as for the case of **1**. The similarity of the magnetic moments for solutions of **1** and **2** is also consistent with their having similar coordination geometries. We therefore conclude that the glassy toluene EPR spectrum of **2** represents the monomeric and low spin complex [PhBP$_3$]CoBr. The resolved hyperfine coupling in the g$_{||}$ region is in accord with this model ($A_{||} = 88 \times 10^{-4}$ cm^{-1}) as it shows an octet, indicative of coupling to a single cobalt nucleus. If the dimer of **2** were maintained in solution, we would have expected to observe a 15-line splitting pattern. A related EPR study was also performed for the chloride **3**. The polycrystalline and glassy EPR spectra of **3**, shown in Figure 6, parts a and b, respectively, are similar to that of **2**. The major difference is that a readily detectable population of the dimer of **3** appears to be present in glassy toluene at 12 K. The low spin monomer [PhBP$_3$]CoCl, however, is the major species present in the glass even at this low temperature. The additional hyperfine resonances observed in the $g_{||}$ region (~2.2) for **3** are also suggestive of a modest concentration of the triplet {[PhBP$_3$]Co(μ-Cl)}$_2$ in the glassy toluene spectrum, that is super-imposed with the signal expected for [PhBP$_3$]CoCl. The hyperfine coupling for [PhBP$_3$]CoCl is resolvable with $A_{||} = 92 \times 10^{-4}$ cm^{-1}. The temperature dependence of the optical spectrum of **3** is discussed below and lends further support to the suggestion that **3** can dimerize in solution as a function of temperature.

IId. Conversion of Low Spin Iodide, 1, to the High Spin Complexes [PhB(CH$_2$P(O)Ph$_2$)$_2$(CH$_2$PPh$_2$)]CoI and [PhBP$_3$]-

(46) Swalen, J. D.; Gladney, H. M. *IBM J. Res. Dev.* **1964**, *8*, 515−526.
(47) van Veen, G. *J. Magn. Resonance* **1978**, *30*, 91−109.
(48) (a) Pilbrow, J. R. *Transition Ion Electron Paramagnetic Resonance*; Clarendon Press: Oxford, 1990. (b) Aasa, R.; Vänngård, T. *J. Magn. Resonance* **1975**, *19*, 308−315.

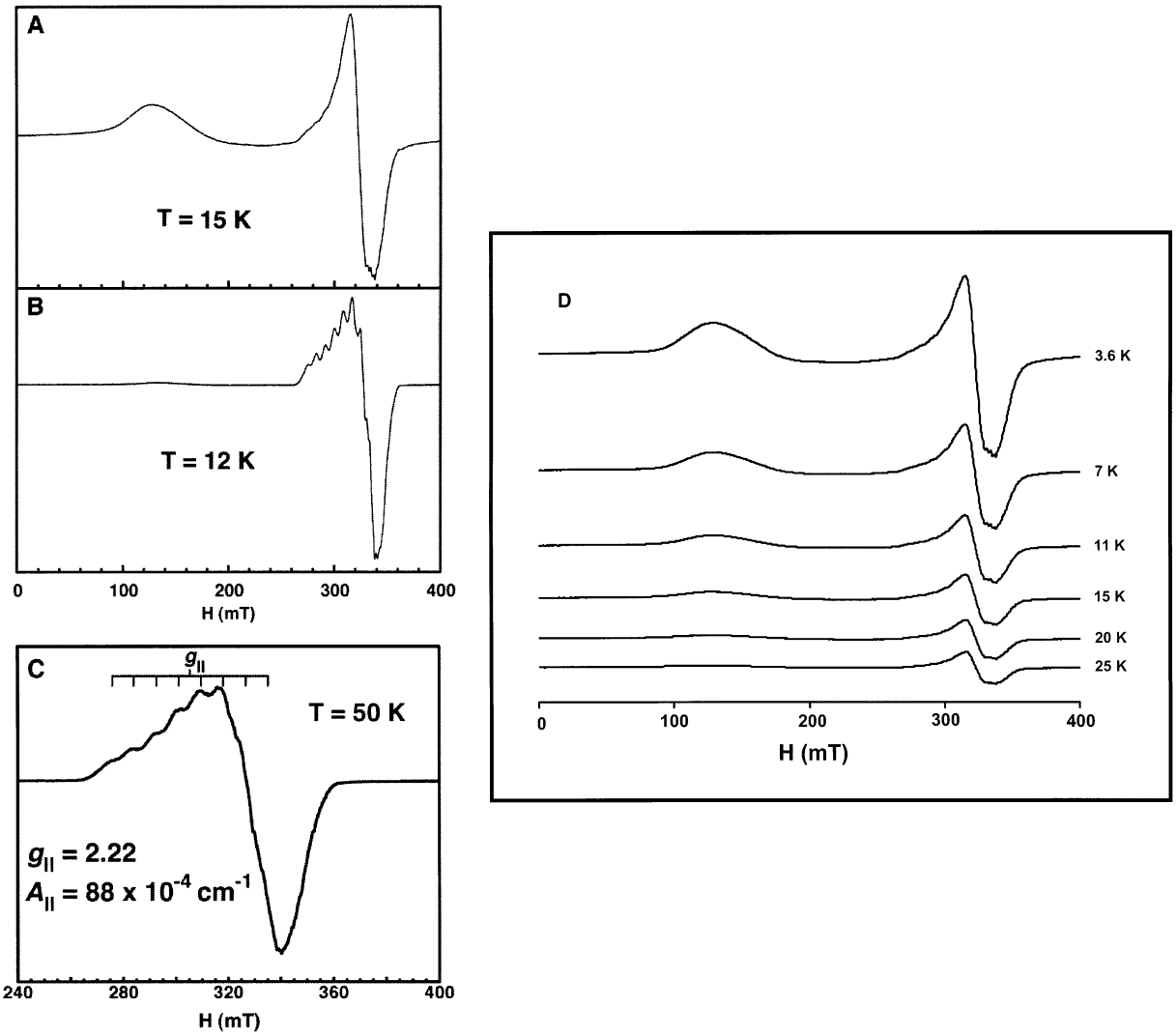

Figure 5. (A) EPR spectrum of a polycrystalline sample of $\{[PhBP_3]Co(\mu\text{-}Br)\}_2$ (15 K). Instrumental parameters: $\nu = 9.480$ GHz, modulation frequency = 100 kHz, modulation amplitude = 4 G, microwave power = 1.01 mW, conversion time = 163.84 ms, time constant = 40.96 ms, 10 scans. (B) EPR spectrum of a glassy toluene solution of $\{[PhBP_3]Co(\mu\text{-}Br)\}_2$ at 12 K. Instrumental parameters: $\nu = 9.472$ GHz, modulation frequency = 100 kHz, modulation amplitude = 4 G, microwave power = 0.101 mW, 1 scan. (C) EPR spectrum of a glassy toluene solution of $\{[PhBP_3]Co(\mu\text{-}Br)\}_2$ at 50 K. $g_{||}$ and $A_{||}$ were estimated by simulating the EPR spectrum. Instrumental parameters: $\nu = 9.477$ GHz, modulation frequency = 100 kHz, modulation amplitude = 5 G, microwave power = 2.02 mW, conversion time = 20.48 ms, time constant = 5.12 ms, 20 scans. (D) Series of EPR spectra for a polycrystalline sample of $\{[PhBP_3]Co(\mu\text{-}Br)\}_2$ plotted to show the temperature dependence of the EPR signal. The signal amplitude increases as the temperature decreases, suggestive of a ferromagnetic triplet ground state.

Co(O-2,6-Me$_2$-C$_6$H$_4$). It was prudent to prepare one or more complexes of similar geometry to **1** with a high spin ground state so that the relevant structural, magnetic, and spectroscopic data could be compared to the monomeric low spin derivatives already described.

The oxygen sensitivity of the halides **1**, **2**, and **3** encouraged us to assess the stoichiometric reaction between **1** and molecular oxygen. We were fortunate to find that the addition of either stoichiometric or excess dioxygen to a benzene solution of **1** resulted in a rapid color change from green to bright blue. The product, which formed quantitatively according to optical and ^{1}H NMR spectroscopies, proved to be a 4-coordinate cobalt iodide complex whose tripodal borate ligand had undergone a 4-electron oxidation process (Scheme 3).[36] The solid-state structure of the product, $[PhB(CH_2P(O)Ph_2)_2(CH_2PPh_2)]CoI$, (**4**), shown in Figure 7A, has approximate C_s symmetry with a mirror plane bisecting the two phosphine oxide donors. By comparison to its green precursor **1**, blue **4** has several structural features

Scheme 3

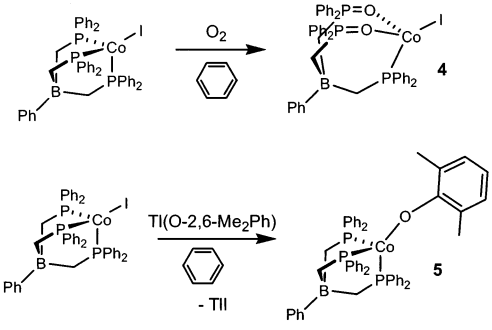

worth highlighting. The Co−I and Co−P bond lengths are appreciably elongated in **4** by comparison to **1**, qualitatively consistent with an expanded high spin cobalt radius (vide infra). Furthermore, the borate counteranion of the oxidized ligand is tethered further away from the cobalt center in **4** (Co−B distance is 3.77 Å in **4** and 3.49 Å in **1**). This fact, coupled with a

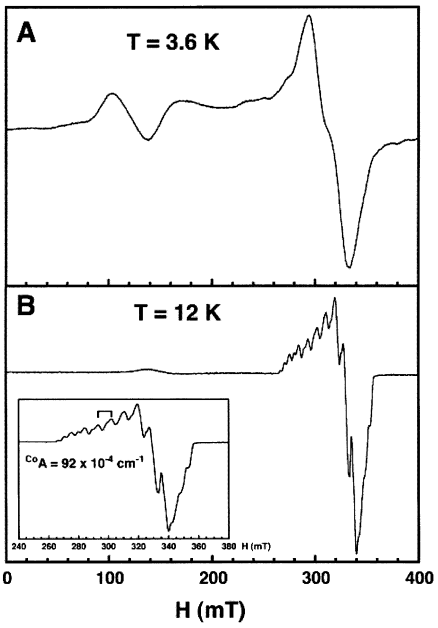

Figure 6. (A) EPR spectrum of a polycrystalline sample of {[$PhBP_3$]Co(μ-Cl)}$_2$ at 3.6 K. Instrumental parameters: ν = 9.477 GHz, modulation frequency = 100 kHz, modulation amplitude = 4 G, microwave power = 0.101 mW, conversion time = 163.84 ms, time constant = 40.96 ms, 4 scans. (B) EPR spectrum of a glassy toluene solution of {[$PhBP_3$]Co(μ-Cl)}$_2$ at 12 K. Instrumental parameters: ν = 9.476 GHz, modulation frequency = 100 kHz, modulation amplitude = 4 G, microwave power = 0.202 mW, conversion time = 163.84 ms, time constant = 40.96 ms, 7 scans. The inset $g \approx 2$ region showing resolved cobalt hyperfine structure; $g_{||}$ and $A_{||}$ were estimated by simulating the EPR spectrum.

decrease in the donor strength of the [$PhB(CH_2P(O)Ph_2)_2(CH_2PPh_2)$] ligand by comparison to its non-oxidized [$PhBP_3$] precursor, suggests that the cobalt center in **4** should experience a weaker ligand-field than its precursor complex **1**. The bromide and chloride complexes appear to undergo an analogous ligand oxidation reaction on exposure to oxygen, though the products were not characterized crystallographically. Green solutions of **2** and **3** rapidly turned blue, and their optical spectra changed accordingly. As alluded to above, partial oxidation of samples of **1**, **2**, and **3** is readily discerned by EPR spectroscopy.

We also prepared a more conventional, 4-coordinate and *high-spin* complex supported by an intact [$PhBP_3$] ligand. The iodide complex **1** was allowed to react with the moderately bulky thallium aryloxide reagent Tl(O-2,6-Me_2Ph), which smoothly generated the aryloxide species [$PhBP_3$]Co(O-2,6-Me_2Ph), (**5**), as a red-brown, crystalline solid (Scheme 3). The solid-state structure of **5**, depicted in Figure 7b, reveals **5** to be monomeric, but grossly distorted from idealized 3-fold symmetry. Each of the three O−Co−P angles is quite different (134.9(1)°, 120.4(1)°, and 105.3(1)°) and one of the phosphine donor arms is slightly elongated by comparison to the other two (2.366(1) Å versus 2.332(1) and 2.343(1) Å, respectively). High spin, 4-coordinate cobalt(II) systems typically adopt higher symmetry when possible; the distorted structure obtained for **5** likely results from steric interactions between the bulky aryloxide and [$PhBP_3$] ligands. The Co−P bond lengths in **5** are, on average, appreciably elongated in comparison to **1** (∼0.12 Å). This difference again qualitatively reflects their different spin states.

IIe. Comparative Magnetic and EPR Characterization of [$PhB(CH_2P(O)Ph_2)_2(CH_2PPh_2)$]CoI (4) and [$PhBP_3$]Co(O-2,6-$Me_2$-$C_6H_4$) (5). The SQUID data obtained for blue **4**, shown in Figure 2, parts a and b, establish it to be a typical high spin cobalt(II) complex. The average magnetic moment of 4.29 μ_B, obtained from the solid-state SQUID data fit between 10 and 300 K, falls within the range of the many 4-coordinate, non square planar high spin systems that have been previously described.[38] A solution moment of 4.5 μ_B (C_6D_6, 25 °C) was estimated by the method of Evans for **4**. The EPR spectrum of **4** also reveals its formal change in spin state upon ligand oxidation. Both low-temperature powder (Figure 8) and glassy toluene samples of **4** gave rise to similar EPR spectra that were distinct from those obtained for **1** and similar to those normally observed for high spin cobalt(II) systems.[37] The intense signal ($g \approx 4.8$) characteristic of **4** was also observed when **2** and **3** were exposed to increasing amounts of oxygen (see Supporting Information), suggesting that similar products are formed in each of the three cases. It is emphasized that the EPR spectrum of **4** was only observed at low temperature (<50 K), typical of high spin cobalt(II) derivatives and contrasting the

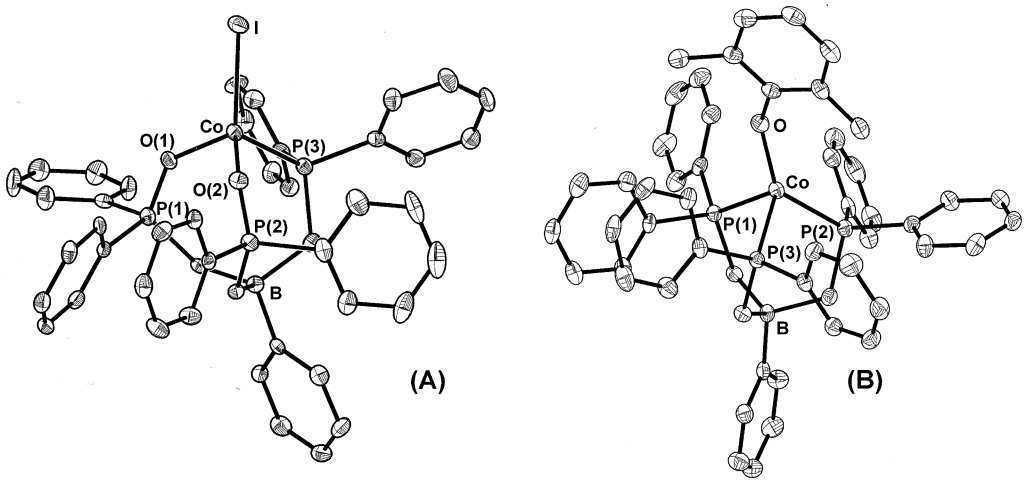

Figure 7. Displacement ellipsoid representation (50%): **(A) [$PhB(CH_2PPh_2)(CH_2P(O)Ph_2)_2$]CoI, (4)**; Selected interatomic distances (Å) and angles (deg): Co−P(3), 2.335(1); Co−I, 2.566(1); Co−O(1), 1.937(2); Co−O(2), 1.937(2); Co−B, 3.768(4); O(1)−P(1), 1.513(2); O(2)−P(2), 1.514(2); O(1)−Co−O(2), 103.3(1); O(1)−Co−I, 117.25(7); O(1)−Co−P(3), 105.90(7); O(2)−Co−I, 115.55(7); P(3)−Co−I, 113.83(3); O(2)−Co−P(3), 98.85(7). **(B) [$PhBP_3$]Co(O-2,6-dimethylphenyl), (5).** Selected interatomic distances (Å) and angles (deg): Co−O, 1.851(2); Co−P(3), 2.332(1); Co−P(2), 2.366(1); Co−P(1), 2.343(1); Co−B, 3.446(3); O−Co−P(3), 120.39(5); O−Co−P(2), 134.93(5); P(3)−Co−P(2), 98.27(2); O−Co−P(1), 105.27(5); P(3)−Co−P(1), 92.72(2); P(2)−Co−P(1), 94.22(2).

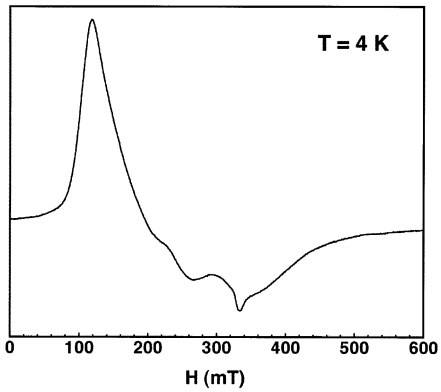

Figure 8. Frozen solution EPR spectrum of [PhB($CH_2P(O)Ph_2$)$_2$(CH_2PPh_2)]-CoI (toluene, 4 K). Instrumental parameters: ν = 9.477 GHz, modulation frequency = 100 kHz, modulation amplitude = 10 G, microwave power = 2.02 mW, conversion time = 40.96 ms, time constant = 10.24 ms, 5 scans.

spectrum of **1**, where a strong isotropic signal was detected even at room temperature. The aryloxide complex **5** also appears to be a high spin species in the solid-state, as evident from its SQUID data provided in Figure 2. Its high spin moment was maintained in solution (4.3 μ_B, C_6D_6, 25 °C). It is also interesting to note that the $\chi_m T$ versus T plot for **5** (see Supporting Information) reveals an unexpected rise in $\chi_m T$ as the sample temperature is lowered. This rise becomes more dramatic at temperatures < 100 K and reaches a maximum at 16 K, at which point it falls precipitously to zero as the temperature is lowered further, perhaps suggestive of intermolecular antiferromagnetic exchange. The glassy toluene EPR spectrum of **5** is also provided in the Supporting Information. Its EPR signal is not detected at elevated temperatures (>50 K).

IIf. Comparative Optical Spectra of [PhBP$_3$]CoI (1), {[PhBP$_3$]CoBr}$_2$ (2), {[PhBP$_3$]CoCl}$_2$ (3), and [PhB($CH_2P(O)Ph_2$)$_2$(CH_2PPh_2)]CoI (4). The room-temperature optical spectra for green solutions of **1**, **2**, and **3** (250−1500 nm), and for the high spin complex **4**, were obtained in toluene and are shown in Figure 9. The spectra for the halides **1**, **2**, and **3** are very similar and are dominated by an apparent broad charge-transfer band in the visible region that displays an expected blue shift from I^- (638 nm) to Br^- (612 nm) to Cl^- (594 nm). Lower energy features that show less halide dependence are also present in the spectrum of each of the three halides. It is important to note that incubation of green toluene solutions of **1** and **2** at −78 °C did not effect an appreciable color change. In contrast, incubation of a green solution of chloride **3** at −78 °C gave rise to a distinctly purple solution whose green color was recovered on warming. The inset spectrum shown in Figure 9 was acquired upon rapid removal of the purple solution containing **3** from a −78 °C cold bath. In accord with the EPR data, we presume that this spectrum represents a superposition of the spectrum for the dimeric form of **3** and its monomeric, pseudo-tetrahedral low spin form. The optical spectrum of high spin **4** is consistent with related tetrahedral and distorted tetrahedral cobalt(II) complexes.[38] The visible region of the spectrum of **4** displays moderately intense bands in the range 580 to 700 nm. A lower energy, broad band is observed ∼1020 nm. Theopold reported similar features for the optical spectrum of a blue, tris(pyrazolyl)borate-supported cobalt(II) iodide monomer in a distorted tetrahedral geometry.[26] The optical spectrum of high spin **5** was also obtained in toluene solution. The visible region of its spectrum was characterized by broad

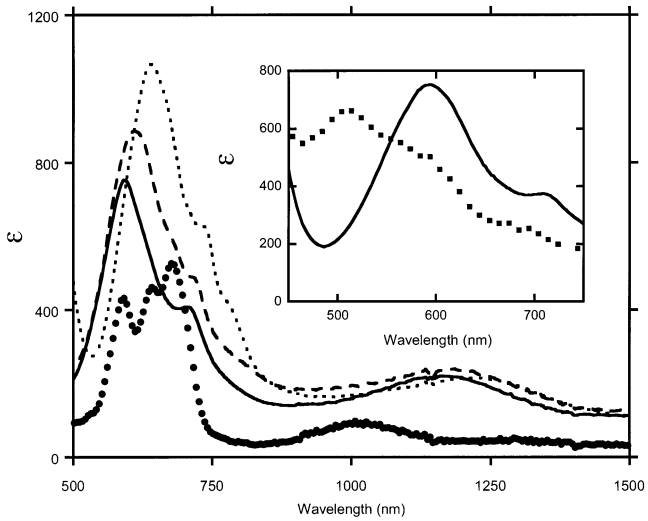

Figure 9. Absorption spectra for compounds [PhBP$_3$]CoI, **1**, (···), {[PhBP$_3$]-Co(μ-Br)}$_2$, **2**, (− − −), {[PhBP$_3$]Co(μ-Cl)}$_2$, **3**, (—), [PhB(CH_2PPh_2)-($CH_2P(O)Ph_2$)$_2$]CoI, **4**, (●) between 500 and 1500 nm. The similarity between each of the spectra suggests that each complex is predominantly monomeric at ambient temperature in toluene solution. **Inset:** {[PhBP$_3$]-Co(μ-Cl)}$_2$, **3**, at 298 K (—) and at 220 K (■) in toluene solution, illustrating the temperature dependence of its optical absorption that is associated with a monomer (298 K) to dimer (220 K) equilibrium.

features between 400 and 800 nm with resolvable maxima at 530, 580, and 752 nm.

III. Discussion

The preceding sections have presented structural, magnetic, and spectroscopic evidence to suggest that a low spin formulation is correct for *monomeric* [PhBP$_3$]CoX systems, where X represents the halides I^-, Br^-, or Cl^-. Although the iodide complex **1** is a simple, 4-coordinate monomer both in the solid-state and in solution, the chloride **3**, and to a lesser extent the bromide **2**, are capable of dimerizing to a modest degree in solution at low temperature; they both crystallize in the dimeric form. The solid-state SQUID and EPR data collected for the dimers **2** and **3** prompt us to assign them to triplet ground states exhibiting weak ferromagnetic coupling. A more detailed analysis of their electronic structures is worth pursuing in future studies, though it is at present clear that the electronic structures of **2** and **3** are quite distinct from the structurally related dimers of Sacconi, these latter systems being characterized by singlet ground states due to pronounced antiferromagnetic exchange.[15]

At room temperature, both **2** and **3** are *predominantly monomeric* in solution.[39] Room-temperature solutions of **1**, **2**, and **3** in toluene are bright green; solutions of **1** and **2** remain green on cooling to 195 K, whereas a solution of **3** turns purple (reversibly) as it is cooled, indicative of the dimer concentration at low temperature. The solution EPR spectra are also consistent with this model. At low temperatures (<50 K), the EPR spectra of iodide **1** and bromide **2** show only the monomer form. For the chloride **3**, however, the dimeric form also appears to be present below 50 K, superimposed with the spectrum for the monomer. The optical spectra for the three complexes are in accord with these data. Each of the spectra shows very similar features at room temperature, suggesting analogous stereochemical environments in solution. Cooling the solution of **3** causes a dramatic change in color from green to purple, reflecting the increase in concentration of its dimeric form.

The most intriguing observation concerns the low spin character of the monomeric form of these simple halide complexes. Configurational solution equilibria between high and low spin complexes of cobalt were first observed more than three decades ago.[8,40,41] The typical situation is as follows: a low spin pentacoordinate cobalt(II) complex can dissociate one ligand to afford a (i) high spin, tetrahedral or distorted tetrahedral structure type, or (ii) a low spin, square planar or distorted square planar structure type. In certain cases, a solution equilibrium has been observed between strictly quadri-coordinate structures that are high spin (tetrahedral) and low spin (square planar), such as the bis(β-ketoamino)cobalt(II) complexes described by Holm and Everett.[8a] Stereochemical tuning of a series of tropocoronand ligands coordinated to divalent cobalt by Lippard and co-workers was shown to give rise to a range of intermediate structure types that were classified as either distorted tetrahedral (and high spin) or distorted square planar (and low spin).[9] The halides described in the present manuscript are anomalous in that, for complexes **2** and **3**, solution equilibria between a low spin, 5-coordinate, distorted square pyramidal structure and a low spin, 4-coordinate, distorted tetrahedral structure apparently exist. The X-ray crystal structure of the iodide complex **1** provides a structural snapshot of the distorted tetrahedral, low spin 4-coordinate structure, a structure that is not directly observable for complexes **2** and **3**, but which is inferred from the solution data available for these complexes. It becomes apparent that a low spin state for quadri-coordinate cobalt(II) can be achieved by a distortion strikingly different from the severe distortion that takes a tetrahedral structure to a square planar structure. In the present case, a more subtle distortion, one that is distinctly axial in character, gives rise to the low spin configuration. The following discussion, accompanied by Figures 10 and 11, provides a simple orbital explanation for this phenomenon.

A tetrahedral ligand-field for divalent cobalt places three degenerate orbitals, the *t* set, at a significantly higher energy than the nonbonding *e* set. Following Hund's rule, four electrons fill the *e* set, and three electrons fill the *t* set, one per orbital in a spin-aligned fashion. As is well-known, this is the origin of the typically observed quartet ground state that has been previously observed for tetrahedral and distorted tetrahedral cobalt(II) complexes. Breaking the symmetry, whether to C_3, C_s, or C_1, does not typically change this situation.[42] The three orbitals at higher energy are only modestly split as the symmetry of the molecule descends from the tetrahedron. This splitting of the degenerate *t* set is typically small by comparison to the pairing energy that would be required to achieve a low spin state. However, if this splitting becomes large, and if an orbital of a_1 symmetry (predominantly z^2) from the upper set is strongly stabilized on distortion, it should be possible to access a low-spin population. We think that the stereochemical environment and the strong ligand-field-donor-strength provided by the [$PhBP_3$] anion achieves this extreme and thereby provides access to the low spin ground state for pseudotetrahedral cobalt(II). The phosphine ligands of [$PhBP_3$] are good sigma-donors and should contribute to a strong ligand-field in pseudo-C_3 **1** whereby the upper orbital set, σ^* in character, lies well above the lower nonbonding orbital set. The dominant factor to consider is the extent to which a hybrid a_1 orbital (predominantly z^2 with some admixed *s* and p_z) is stabilized as the cobalt center

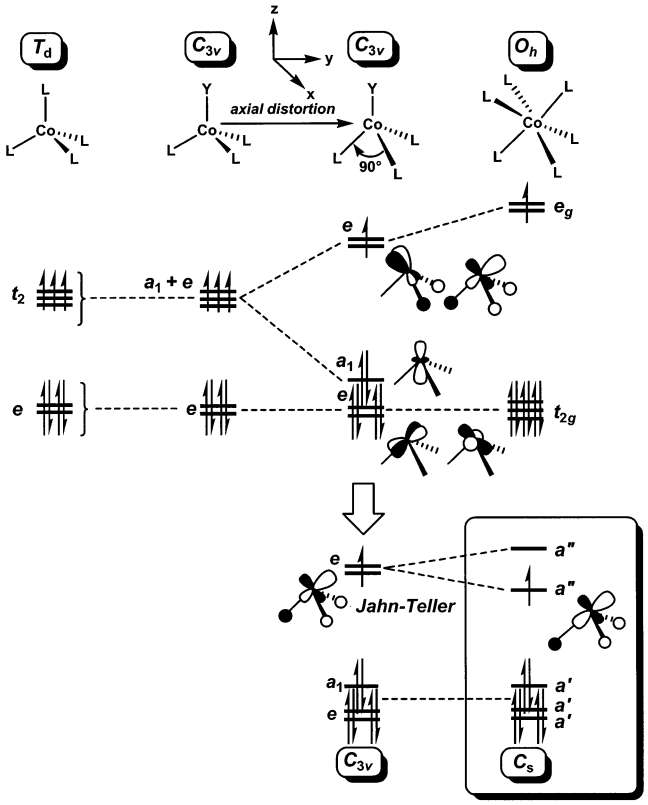

Figure 10. Qualitative d-orbital splitting diagram that depicts a descent in symmetry from T_d to C_{3v} symmetry for an axially distorted tetrahedral cobalt(II) system. As defined, the *z*-axis proceeds through one Co−L vector of the starting tetrahedron. The figure presents three limiting structure types: an idealized tetrahedron (CoL_4), a C_{3v} structure ($CoYL_3$) with bond angles analogous to the tetrahedral structure, and a C_{3v} structure resulting from a strong axial distortion ($CoXP_3$) in which the P−Co−P angle are fixed to ∼90 °. Note that this descent proceeds naturally from an octahedral CoL_6 species but that the correlation diagram places the *z*-axis at the center of one face of the octahedron rather than its typical position directly along one of the L−Co−L axes. The atomic compositions under O_h symmetry for the t_{2g} and e_g set under this axis definition are as follows:[49] **For t_{2g}:** z^2; $\{(2/3)^{1/2}(x^2 - y^2) - (1/3)^{1/2}yz\}$; $\{(2/3)^{1/2}xy - (1/3)^{1/2}xz\}$. **For e_g:** $\{(1/3)^{1/2}x^2 - y^2 + (2/3)^{1/2}yz\}$; $\{(1/2)^{1/2}xy + (2/3)^{1/2}xz\}$. The lower portion of Figure 10 extends the splitting diagram to C_s symmetry by a Jahn−Teller distortion that elongates one donor ligand and places the single unpaired electron in a nondegenerate orbital stabilized by a lowering in σ^* character of one of the orbitals from the formally degenerate σ^* e-set.

is axially distorted along the Co−I vector (i.e., along *z*). When stabilization of this a_1 orbital becomes strong enough, and when the ligand-field is sufficiently strong so as to destabilize the now high-lying *e*-set, electron pairing becomes energetically favorable and a low spin ground state is achieved. Figure 10 summarizes this model schematically by correlating the low spin configuration in idealized C_{3v} symmetry to idealized T_d and O_h structures. Note that the natural choice of coordinate axes for all of the structures shown in Figure 10 places the *z*-axis through one face of an octahedral ML_6. Although this definition of axes is obvious for C_{3v} symmetry, it is not the typical choice for O_h ML_6. To describe the orbital character of the lower t_{2g} and upper e_g sets, the orbital functions need to be correlated to the new coordinate axis system. For an O_h ML_6 complex, these functions transform as:[49] **t_{2g} set:** z^2; $\{(2/3)^{1/2}(x^2 - y^2) - (1/3)^{1/2}yz\}$; $\{(2/3)^{1/2}xy - (1/3)^{1/2}xz\}$. **For e_g set:** $\{(1/3)^{1/2}x^2 - y^2 + (2/3)^{1/2}yz\}$; $\{(1/2)^{1/2}xy + (2/3)^{1/2}xz\}$. When the axial

(49) Orgel, L. E. *An Introduction to Transition-Metal Chemistry*; Wiley: New York, 1960; p 174.

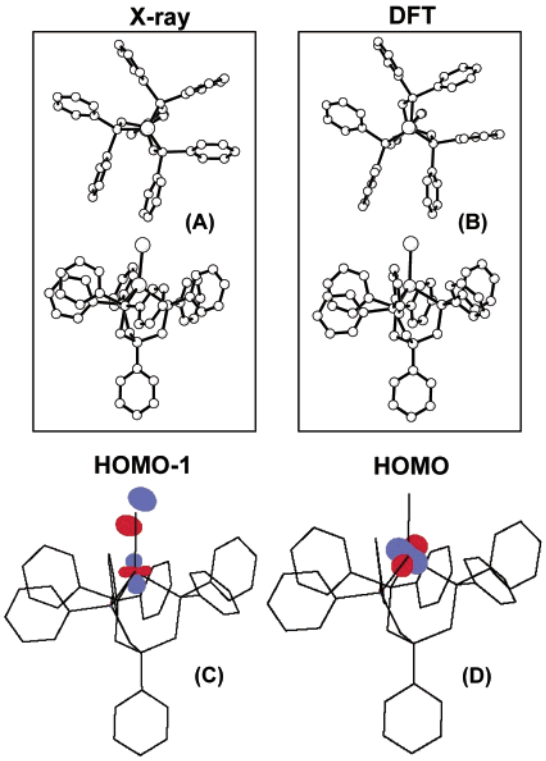

Figure 11. Figure shows the experimental (X-ray) **(A)** and calculated (DFT) **(B)** molecular structures for complex **1**. Representations of the HOMO-1 **(C)** and HOMO **(D)** orbitals obtained from the DFT electronic structure calculations are also shown. The calculated (DFT) bond distances (Å) and angles (deg) were theoretically determined to be as follows. The experimentally determined value is shown in parentheses: Co−I, 2.585 (2.474); Co−P(1), 2.282 (2.163); Co−P(2), 2.240 (2.208); Co−P(3), 2.402 (2.244); P(1)−Co−P(2), 88.6 (90.5); P(1)−Co−P(3), 96.0 (92.9); P(2)−Co−P(3), 90.5 (92.3); P(1)−Co−I, 119.0 (119.6); P(2)−Co−I, 131.6 (127.3); P(3)−Co−I, 121.6 (124.6).

distortion is so severe that the angle (L−Co−L) between the three fac ligands becomes 90°, enforced in complex **1** by the [$PhBP_3$] ligand, the set of orbitals derived for O_h symmetry correlate very well with the axially distorted pseudo-tetrahedral structure type. For a low spin configuration we anticipate a Jahn−Teller distortion from C_{3v} to C_s symmetry. The lower portion of Figure 10 depicts this situation and suggests that the final ground electronic configuration (using the functions given above) to be $(\{(2/3)^{1/2}(x^2 - y^2) - (1/3)^{1/2}yz\})^2(\{(2/3)^{1/2}xy - (1/3)^{1/2}xz\})^2(z^2)^2(\{(1/3)^{1/2}x^2 - y^2 + (2/3)^{1/2}yz\})^1(\{(1/2)^{1/2}xy + (2/3)^{1/2}xz\})^0$. The EPR spectrum of **1** ($g_{||} = 2.20$ and $g_{\perp} = 2.05$) is consistent with this configuration to the extent that $g_{||}$ is appreciably higher than the free electron value, suggesting that the unpaired spin is not localized in an orbital of z^2 parentage. Rather, the unpaired spin resides in an orbital that is formally $\{(1/3)^{1/2}x^2 - y^2 + (2/3)^{1/2}yz\}$ within the present coordinate axis scheme.

Hoping to corroborate this conclusion we performed a theoretical electronic structure calculation on the title complex **1**. The geometry of the complete complex, including the aryl rings of the [$PhBP_3$] ligand, was theoretically determined by performing a geometry optimization that used the experimentally determined structural coordinates for **1** as a starting point (see the Experimental Section for details). The structure calculation converged and reasonable, though not excellent, agreement between the theoretical structure of **1** and its experimentally determined structure was established (see Figure 11, parts a and b). The electronic structure of **1** determined by DFT suggests the HOMO orbital to be one of π-antibonding character between the cobalt center and the iodide ligand, and the HOMO-1 orbital to be predominantly dz^2 in character, in accord with the qualitative MO scheme presented in Figure 10.

Although a great many high spin distorted tetrahedral complexes are known, two systems that deserve to be singled out with respect to the present discussion are the monomeric halides [Tp′′]CoI ([Tp′′] = hydrotris(3-*tert*-butyl-5-methylpyrazolyl)-borate) and [PhTt$^{tert\text{-}butyl}$]CoX ([PhTt$^{tert\text{-}butyl}$] = phenyl(tris(*tert*-butylthio)methyl)borate, X = Cl^- or I^-), each of which has been structurally characterized and assigned as high spin.[26,27] Like complex **1**, they each have approximate C_3 symmetry, and like complex **1**, they have a borate atom placed in close proximity to the cobalt center along the *z*-axis. The X-ray structures of [Tp′′]CoI and [PhTt$^{tert\text{-}butyl}$]CoX also show a rather strong distortion in the axial direction (the average I−Co−N angle is ∼122° for [Tp′′]CoI; the average Cl−Co−S angle is ∼118° for [PhTt$^{tert\text{-}butyl}$]CoCl and ∼118° for [PhTt$^{tert\text{-}butyl}$]CoI). Geometric constraints for the facially capping [$PhBP_3$], [Tp′′], and [PhTt$^{tert\text{-}butyl}$] donor ligands enforce the large X−Co−L (L = P, N, and S donor, respectively) bond angles in each case. As previously mentioned, low spin **1** is somewhat distorted from C_3 symmetry by elongation of one of the phosphine donors. A similar distortion is not observed in [Tp′′]CoI, nor in [PhTt$^{tert\text{-}butyl}$]CoCl and [PhTt$^{tert\text{-}butyl}$]CoI. In these three cases, the three Co−L (L = N, S) bond lengths are very similar and the three X−Co−L bond angles show little variation. The solid-state structure of **1** is a reasonable consequence of its low spin configuration, expected to give rise to a Jahn−Teller distortion. That the related complexes [Tp′′]CoI, [PhTt$^{tert\text{-}butyl}$]CoCl, and [PhTt$^{tert\text{-}butyl}$]CoI do not adopt a low spin configuration and show a similar Jahn−Teller distortion likely reflects the relative ligand-field donor strengths of the three borate-derived donor ligands. The upper lying e-set (in C_{3v}) is σ^*. Its degree of destabilization should directly reflect the relative donor strength of three donor ligands. The [$PhBP_3$] ligand appears to be the strongest donor, destabilizing the upper orbital set to the greatest extent, but by a relative amount that has yet to be quantified. The ability of each ligand to accommodate a Jahn−Teller distortion (if a low spin configuration is to occur), however, is also a variable that needs to be considered. Tris(pyrazolyl)borate ligands, when coordinated in an η^3-fashion, are not very flexible. Geometric JT-distortion to a stable low spin configuration might therefore be energetically unfavorable. Thus, [Tp]-derived ligands could provide a ligand-field strength similar to [$PhBP_3$], but still be coordinatively less flexible, thereby raising the energy of the doublet state above the quartet state for [Tp]CoX derivatives. Riordan's [PhTt$^{tert\text{-}butyl}$]CoX system is another matter. That the monomeric complexes [PhTt$^{tert\text{-}butyl}$]CoX are high spin is somewhat surprising based on the electronic scheme presented herein. It would seem that the tris(thioether)borate ligands are flexible enough to permit the Jahn−Teller distortion. The high-spin character of the [PhTt$^{tert\text{-}butyl}$]CoX derivatives is perhaps reflective of their less pronounced axial elongation and their attenuated ligand-field strength by comparison to the [$PhBP_3$]CoX systems. This would have the effect of narrowing the gap between the a_1 orbital and the upper *e* manifold, thereby making the high spin configuration of (PhTt$^{tert\text{-}butyl}$)CoX complexes more stable. It would certainly be of interest to

comparatively study the temperature dependence of the magnetic behavior of Theopold's and Riordan's cobalt(II) systems by SQUID magnetometry to establish whether any of the low spin form for these complexes is populated at very low temperatures.

An interesting observation for the low spin complexes **1**, **2**, and **3** is that they bind a stoichiometric equivalent of CO readily to form the low spin, 5-coordinate carbonyl adducts [$PhBP_3$]-Co(CO)(X) (X = I^-, Br^-, Cl^-). Although a full discussion of these and related 5-coordinate [$PhBP_3$]Co(II) complexes will be provided elsewhere,[43] it is of interest in the present discussion to compare the relative CO donor strength of [$PhBP_3$]Co(CO)-(Br) to the isostructural but cationic complex [{$CH_3C(CH_2$-$PPh_2)_3$}Co(Br)(CO)][BPh_4] previously reported by Sacconi.[23d] The carbonyl stretching frequency of structurally characterized [$PhBP_3$]Co(CO)(Br) is 2030 cm^{-1}. The carbonyl stretching frequency of structurally characterized [{$CH_3C(CH_2PPh_2)_3$}-Co(Br)(CO)][BPh_4] is 2060 cm^{-1}. That the cationic complex exhibits a CO stretch 30 cm^{-1} higher in energy than the neutral derivative suggests that the anionic borato ligand is an appreciably stronger donor than its neutral ligand counterpart. The increased donor strength likely accounts for the tendency of dimeric bromide **2** to dissociate to a 15 electron, low spin monomer in solution. Such an equilibrium has not been observed for any of the cationic cobalt(II) dimers supported by triphos, in which a halide or pseudohalide occupies the bridging position.[23,24] We highlight this distinction because it is important to bear in mind with respect to the degree of "zwitterionic" character ascribed to neutral complexes supported by (phosphino)borate ligands. From the perspective of a simple Lewis structure depiction, simple resonance contributors that delocalize the anionic borate charge to the phosphine donor ligands are not available. This contrasts the situation for tris(pyrazolyl)-borate ligands, where simple resonance delocalization is expected to partially distribute the negative charge to the N-donor atoms. That [$PhBP_3$] is such a strong field donor, however, suggests that there is appreciable communication between the borate anion and the bound metal center, either through space or through the sigma framework. Our ability to identify low spin, monomeric cobalt(II) halides that do not irreversibly dimerize might be a direct consequence of the strong field of the [$PhBP_3$] anion: it stabilizes complexes that are formally electron deficient. The high spin complexes **4** and **5** are also monomeric, as are the high spin systems of Theopold and Riordan.[26,27] This is perhaps to be anticipated, as they do not possess an empty *d* orbital to accommodate the lone pair of a bridging halide ligand. In accord with this model, we note that the high spin cobalt(II) derivatives **4** and **5**, in addition to the Riordan and Theopold systems, appear to be more resistant to coordination of carbon monoxide. This fact may, however, simply reflect other factors such as relative ligand-field donor strengths and, for the case of **5** in particular, steric considerations.

IV. Conclusion

In summary, we have synthesized and studied a series of divalent cobalt complexes supported by the [$PhBP_3$] anion. Structural, magnetic, and spectroscopic data for each of these systems is suggestive of low spin behavior for their monomeric, distorted tetrahedral structure types. The low spin nature of the monomeric form of these halides appears to be unique from related systems that have been previously studied. Two scenarios that transform a high spin, 4-coordinate tetrahedral complex to a 4-coordinate species that is low spin can therefore be put forward. The first scenario pertains to the traditional case in which a high spin tetrahedral structure is distorted to a low-spin square planar structure type. The second scenario, that which is described herein, occurs when coupling of a strong ligand-field donor strength with a pronounced axial distortion leads to a distorted tetrahedral geometry that can accommodate a cobalt(II) ion in a low spin ground-state configuration. The latter, more gentle distortion exposes an orbital at the cobalt(II) center appropriate for small molecule binding, a feature that could be exploited if tunable crossover systems for 4-coordinate cobalt(II) prove accessible. We are pursuing this possibility by searching for new [$PhBP_3$]CoX systems that display spin-crossover phenomena while maintaining 4-coordination in an approximate tetrahedral structure type. We are also pursuing new tris(phosphino)borate ligands to further test our electronic model.

Experimental Section

All manipulations were carried out using standard Schlenk or glovebox techniques under a dinitrogen atmosphere. Unless otherwise noted, solvents were deoxygenated and dried by thorough sparging with N_2 gas followed by passage through an activated alumina column. Nonhalogenated solvents were typically tested with a standard purple solution of sodium benzophenone ketyl in tetrahydrofuran to confirm effective oxygen and moisture removal. The reagents CoI_2, $CoBr_2$, $CoCl_2$, and $TlPF_6$ were purchased from commercial vendors and used without further purification. The preparation of [$PhBP_3$] has been previously reported.[13] TlO-2,6-Me_2Ph was prepared according to a literature procedure.[44] Elemental analyses were performed by Desert Analytics, Tucson, AZ. A Varian Mercury-300 NMR spectrometer or a Varian Inova-500 NMR spectrometer was used to record ^{1}H NMR spectra at ambient temperature unless otherwise stated. ^{1}H chemical shifts were referenced to residual solvent. Deuterated toluene and benzene were purchased from Cambridge Isotope Laboratories, Inc. and were degassed and dried over activated 3 Å molecular sieves prior to use. UV−vis measurements were taken on a Hewlett-Packard 8452A diode array spectrometer using a quartz crystal cell with a Teflon cap. Near-IR measurements were taken on a Cary 14 spectrophotometer using a quartz crystal cell with a Teflon cap. IR measurements were obtained using a Bio Rad Excalibur FTS 3000 with a KBr solution cell. X-ray diffraction studies were carried out in the Beckman Institute Crystallographic Facility on a Bruker Smart 1000 CCD diffractometer.

Magnetic Measurements. Measurements were recorded using a Quantum Designs SQUID magnetometer running MPMSR2 software (Magnetic Property Measurement System Revision 2). Data were recorded at 5000 G. Samples were suspended in the magnetometer in plastic straws sealed under nitrogen with Lilly No. 4 gel caps. Each measurement was performed on samples that had been recently subjected to combustion analysis to verify their purity. Loaded samples were centered within the magnetometer using the DC centering scan at 35 K and 5000 gauss. Data were acquired at 2−10 K (one data point every 2 K), 10−60 K (one data point every 5 K), 60−310 K (one data point every 10 K).

$$\chi_m = \frac{\chi M}{mG} \quad (1) \qquad \mu_{eff} = \sqrt{7.997\chi_m T} \quad (2)$$

The magnetic susceptibility was adjusted for diamagnetic contributions using the constitutive corrections of Pascal's constants and a fixed temperature independent paramagnetism (TIP) crudely set to 2×10^{-4} cm^3 mol^{-1}.[45] The molar magnetic susceptibility (χ_m) was calculated by converting the calculated magnetic susceptibility (χ) obtained from the magnetometer to a molar susceptibility (using the multiplication

factor {(molecular weight)/[(sample weight)(Field Strength)]}). Curie−Weiss behavior was verified by a plot of χ_m^{-1} versus T (shown in Figures 2b and 3b). Data were analyzed using eqs 1 and 2. Average magnetic moments were taken from the average of magnetic moments from the ranges indicated in the Experimental Section for each complex. The Weiss constant (Θ) was taken as the x-intercept of the plot of χ_m^{-1} versus T. Error bars were established at 95% confidence using regression analysis or taking two standard deviations from the mean. Solution magnetic moments were measured by the method of Evans and were adjusted for diamagnetic contributions using the constitutive corrections of Pascal's constants.[29]

Averaged g-factors can be extracted from the susceptibility data, assuming zero orbital contributions, using the following equation:[45]

$$\chi_m = \frac{Ng^2\beta^2}{3kT}(S(S+1))$$

EPR Measurements. X-band EPR spectra were obtained on a Bruker EMX spectrometer equipped with a rectangular cavity working in the TE_{102} mode. Variable temperature measurements were conducted with an Oxford continuous-flow helium cryostat (temperature range 3.6−300 K). Accurate frequency values were provided by a frequency counter built in the microwave bridge. Solution spectra were acquired in toluene for all of the complexes. Sample preparation was performed under a nitrogen atmosphere, *particularly* important for handling the low spin complexes **1**, **2**, and **3** (note: adventitious oxygen is problematic because it gives rise to a high spin monomer concentration, as in the conversion of **1** to **4**).

EPR simulations for the monomers were performed with the program WINEPR *SimFonia* (Version 1.25, Bruker Analytische Messtechnik GmbH); this software is based on second-order perturbation solution of the spin Hamiltonian: $H = H\cdot g\cdot S + \Sigma\, S\cdot A\cdot I$. For the dimers, the absolute values of the spin-Hamiltonian parameters were extracted from simulations of the EPR spectra. Calculations were carried out on a PC using FORTRAN code based on Gladney's general EPR fitting program,[46] and adapted for simulations of EPR spectra of randomly oriented spin triplets. Transition fields and corresponding average transition moments[47] were computed in the magnetic field domain[48] by matrix diagonalization of the $S = 1$ spin Hamiltonian.

$$\hat{H} = \beta(g_zH_zS_z + g_xH_xS_x + g_yH_yS_y) + D\left(S_z^2 - \frac{3}{2}\right) + E(S_x^2 - S_y^2)$$

D and E are defined in terms of the components of the diagonal fine-structure tensor as follows:

$$D_{zz} = \frac{2}{3}D;\quad D_{xx} = -\frac{1}{3}D + E;\quad D_{yy} = -\frac{1}{3}D - E$$

DFT Calculations. A geometry optimization was performed for complex **1** using Jaguar (Version 4.1) starting from coordinates based on the solid-state structure that had been determined by X-ray diffraction. No symmetry constraints were imposed and the calculation was performed on a doublet electronic state. The method used was B3LYP with LACVP** as the basis set (modified to LACVP**++ for the boron atom). Optimization was considered converged when energy changes in successive iterations fell below 0.3 kcal/mol. It should also be noted that convergence was also achieved for a system when the geometry was optimized assuming a quartet ground state.

Synthesis of [PhBP$_3$]CoI, 1. A benzene solution (50 mL) of the thallium reagent, [PhBP$_3$]Tl, (0.356 g, 0.400 mmol) was added to a stirring suspension of CoI_2 (0.250 g, 0.799 mmol) in benzene (20 mL). After stirring at ambient temperature for 24 h, the resulting green solution was filtered through diatomaceous earth, concentrated in vacuo (50% original volume), and filtered through diatomaceous earth once again. Vapor diffusion of petroleum ether into the resulting green filtrate afforded the pure crystalline product (0.317 g, 91.1%) which was analyzed: ^{1}H NMR (C_6D_6, 300 MHz): δ 22.2 (bs), 15.8 (s), 10.8 (s), 7.7 (s), 7.5 (s), 4.3 (bs), 2.2 (s), −8.5 (s). IR (cm^{-1}): 1433, 1091, 739. UV−vis (C_6H_6) λ_{max}, nm (ϵ): 638 (1112), 738 (627). SQUID (solid − average 30−220K): $\mu_{eff} = 2.65 \pm 0.03\ \mu_B$ $\Theta = -1.43$ K. Evans Method (C_6D_6): 2.76 μ_B. Anal. Calcd for $C_{45}H_{41}BCoIP_3$: C, 62.03; H, 4.74. Found: C, 61.76; H, 4.75.

Synthesis of {[PhBP$_3$]Co(μ-Br)}$_2$, 2. A benzene solution (50 mL) of the thallium reagent, [PhBP$_3$]Tl (0.507 g, 0.570 mmol), was added to a stirring suspension of $CoBr_2$ (0.250 g, 1.14 mmol) in benzene (20 mL). After stirring at ambient temperature for 24 h, the resulting green solution was filtered through diatomaceous earth. The filtrate was pumped to dryness to leave a purple powder that was redissolved in benzene (20 mL), filtered over diatomaceous earth, and again thoroughly dried in vacuo. A UV−vis spectrum of this powder suggested a mixture of products. The powder was redissolved in benzene (5 mL) and filtered over a fine sintered-glass frit. A microcrystalline purple powder precipitated from the solution; this powder (0.132 g, 28.1%) was dried and analyzed: ^{1}H NMR (C_6D_6, 300 MHz): δ 26.7 (bs), 11.0 (s), 7.6 (s), 7.4 (s), 4.2 (bs), 2.2 (s). UV−vis (C_6H_6) λ_{max}, nm (ϵ): 612 (1773), 718 (958). SQUID (solid, average 10−100 K): $\mu_{eff} = 1.77 \pm 0.08\ \mu_B$, $\Theta = -1.48 \pm 0.49$ K; (solid, average 110−310 K) 2.11 μ_B. Evans Method (C_6D_6, calculated for a monomer): 2.6 μ_B. Anal. Calcd for $C_{90}H_{82}B_2Br_2Co_2P_6$: C, 65.56; H, 5.01. Found: C, 65.23; H, 4.87. The sample used for the EPR and SQUID measurements, which was recrystallized two more times, analyzed as follows: C, 65.70; H, 5.04.

Synthesis of {[PhBP$_3$]Co(μ-Cl)}$_2$, 3. A benzene solution (50 mL) of the thallium reagent, [PhBP$_3$]Tl (0.857 g, 0.963 mmol), was added to a stirring suspension of $CoCl_2$ (0.250 g, 1.93 mmol) in benzene (20 mL). After stirring at ambient temperature for 24 h, the resulting green solution was filtered through diatomaceous earth. The filtrate was dried in vacuo to a purple powder that was then redissolved in benzene (20 mL), filtered over diatomaceous earth, and again thoroughly dried. The resulting purple powder was redissolved in benzene (5 mL) and filtered over a fine sintered-glass frit; this caused a microcrystalline purple powder to precipitate from solution. The dried powder (0.195 g, 25.9%) was analyzed: ^{1}H NMR (C_6D_6, 300 MHz): δ 31.9 (bs), 15.0 (s), 11.2 (s), 9.1 (s), 7.7 (s), 7.4 (s), 3.9 (bs), 2.2 (s). UV−vis (C_6H_6) λ_{max}, nm (ϵ): 594 (1507), 712 (724). SQUID (solid − average 10−100 K): $\mu_{eff} = 2.47 \pm 0.14\ \mu_B$, $\Theta = -3.13 \pm 0.67$ K; (solid − average 110−310 K) 2.79 μ_B. Evans Method (C_6D_6, calculated for a monomer): 2.8 μ_B. Anal. Calcd for $C_{90}H_{82}B_2Cl_2Co_2P_6$: C, 69.30; H, 5.30. Found: C, 68.14; H, 5.18. The sample used for the EPR and SQUID measurements, which was recrystallized two more times, analyzed as follows: C, 69.56; H, 5.36.

Alternative Preparation for 2 and 3. Thallium hexafluorophosphate (0.090 g, 0.26 mmol) was added to a stirring THF (20 mL) solution of **1** (0.201 g, 0.231 mmol). A yellow powder precipitated within 5 min and was subsequently removed by filtration through diatomaceous earth. NaCl (0.26 g, 4.4 mmol) was added to the filtrate, and the reaction solution was allowed to stir for 24 h. The above process was then repeated with additional $TlPF_6$ and NaCl. After another 24 h, the salts were removed by filtration; a UV−vis spectrum of the product solution indicated that **1** had been fully consumed, and the spectrum matched that of **3**. The solution was concentrated in vacuo to 50% of its original volume and allowed to stand for 24 h. White precipitate (NaCl) was removed by filtration, and the green solution was concentrated to dryness, redissolved in benzene, and once again allowed to stand for 12 h. Repeated filtration through diatomaceous earth ensured complete removal of salts. The final product was obtained by drying thoroughly in vacuo to afford purple **3** as a fine powder (0.159 g, 88.6%). An analogous protocol was effective for converting **1** to **2**, in this case using KBr instead of NaCl. Both UV−vis and ^{1}H NMR spectroscopies are useful in monitoring the metathesis procedure to ensure complete conversion.

Synthesis of [PhB(CH$_2$P(O)Ph$_2$)$_2$(CH$_2$PPh$_2$)]CoI, 4. A 100 mL Schlenk flask with a Teflon stir bar was charged with a benzene (30 mL) solution of **1** (0.278 g, 0.319 mmol) and stirred at room temperature. Oxygen (7.8 mL at 1 atm, 0.32 mmol) was added to the reaction vessel via syringe through a rubber septum. After 4 h, the solution,

which had turned bright blue, was dried in vacuo to a fine blue powder. Washing this powder with petroleum ether (3 × 10 mL) and concentrating it to dryness afforded the final product (0.225 g, 79.1% yield) that was analyzed. ^{1}H NMR (C_6D_6, 300 MHz): δ 16.2 (s), 13.8 (s), 10.1 (s), 9.47 (s), 9.28 (s), 7.90 (s), 7.09 (s), −2.1 (s). UV−vis (C_6H_6) λ_{max}, nm (ϵ): 590 (450), 642 (461), 682 (520). IR (cm^{-1}): 1435, 1126, 1095, 1071, 752. SQUID (solid, average 30−310 K): μ_{eff} = 4.33 ± 0.09 μ_B, Θ = −2.74 K. Evans Method (C_6D_6): 4.4 μ_B. Anal. Calcd for $C_{45}H_{41}BCoIP_3O_2$: C, 59.83; H, 4.57. Found: C, 59.62; H, 4.80.

Synthesis of [PhBP$_3$]Co(O-2,6-dimethylphenyl), 5. A THF solution (5 mL) of the thallium reagent Tl−O-2,6-dimethylphenyl (0.0433 g, 0.133 mmol) was added to a stirring solution (10 mL) of **1** (0.116 g, 0.133 mmol). A yellow precipitate (TlI) formed within 15 min and was removed by filtration through diatomaceous earth. The remaining brown solution was stirred overnight. The reaction volatiles were removed in vacuo and the resulting brown powder was redissolved in benzene. The benzene was lyophilized to thoroughly remove any remaining THF. The resulting fine powder was filtered once more through diatomaceous earth as a benzene (3 mL) solution. Vapor diffusion of petroleum ether into this benzene solution afforded the red-brown, crystalline product (0.067 g, 58.7% yield) that was analyzed. ^{1}H NMR (C_6D_6, 300 MHz): δ 67.0 (s), 52.4 (s), 17.9 (s), 12.4 (s), 11.6 (s), 11. 0 (s), 9.0 (s), 8.45 (s), 7.80 (s), 7.45 (s), 7.06 (s), −3.4 (bs), −6.5 (s), −62.2 (s). UV−vis (C_6H_6) λ_{max}, nm: 534 (1740), 752 (624). SQUID (solid, average 30−310 K): μ_{eff} = 4.36 ± 0.18 μ_B, Θ = 7.48 K. Evans Method (C_6D_6): 4.4 μ_B. Anal. Calcd for $C_{53}H_{50}BCoP_3O$: C, 73.54; H, 5.82. Found: C, 73.32; H, 5.95.

X-ray Crystal Structure Analysis of 1. X-ray quality crystals were obtained by vapor diffusion of petroleum ether into a concentrated solution of **1** in benzene. A dark green crystalline blade was mounted on a glass fiber with Paratone N oil. The structure was solved by direct methods in conjunction with standard difference Fourier techniques. The largest peak and hole in the difference map were 0.775 and −0.614 e.Å^{-3}, respectively. Maximum and minimum transmission were equal to 0.895 and 0.804, respectively. Crystal data for $C_{45}H_{41}BCoIP_3 \cdot {}^1/_2(C_6H_6)$, monoclinic space group $P2_1/c$ (#14), a = 22.5443(17) Å, b = 12.7044(9) Å, c = 29.526(2) Å, β = 90.230(2)°, V = 8456.6(11) Å^3, Z = 8, D_{calcd} = 1.430 g/cm^3, Abs. Coefficient = 1.274 mm^{-1}, Mo−Kα λ = 0.710 73 Å, T = 98 K, Bruker SMART 1000 CCD, crystal size 0.18 × 0.13 × 0.09 mm^3, θ_{max} = 25.55°, $R1$ = 0.0476, $wR2$ = 0.0786 for $I > 2s(I)$, $R1$ = 0.0899, $wR2$ = 0.0843, G_F ($1/\sigma^2$ weighting) = 1.137, number of reflections collected 50716 (−24 = h = 23, −13 = k = 13, −31 = l = 31), number of independent reflections 11 064, number of parameters 926.

X-ray Crystal Structure Analysis of 2. X-ray quality crystals were obtained by vapor diffusion of petroleum ether into a concentrated solution of **2** in benzene. A purple crystalline needle was mounted on a glass fiber with Paratone N oil. The structure was solved by direct methods in conjunction with standard difference Fourier techniques. The largest peak and hole in the difference map were 2.231 and −1.641 e.Å^{-3}, respectively. Maximum and minimum transmission were equal to 0.915 and 0.713, respectively. Crystal data for $C_{90}H_{82}B_2Br_2Co_2P_6$, orthorhombic space group $Pbcn$ (#50), a = 22.214(3) Å, b = 19.286(3) Å, c = 18.008(3) Å, V = 7715.0(19) Å^3, Z = 4, D_{calcd} = 1.419 g/cm^3, Abs. Coefficient = 1.637 mm^{-1}, Mo−Kα λ = 0.71073 Å, T = 98 K, Bruker SMART 1000 CCD, crystal size 0.22 × 0.11 × 0.05 mm^3, θ_{max} = 27.78°, $R1$ = 0.0695, $wR2$ = 0.0965 for $I > 2s(I)$, $R1$ = 0.1432, $wR2$ = 0.1012, G_F ($1/\sigma^2$ weighting) = 1.534, number of reflections collected 9263 (0 = h = 29, 0 = k = 26, 0 = l = 24), number of independent reflections 9263, number of parameters 461.

X-ray Crystal Structure Analysis of 3. X-ray quality crystals were obtained by vapor diffusion of petroleum ether into a concentrated solution of **3** in benzene. A purple crystalline block was mounted on a glass fiber with Paratone N oil. The structure was solved by direct methods in conjunction with standard difference Fourier techniques. The largest peak and hole in the difference map were 0.821 and −0.495 e.Å^{-3}, respectively. Maximum and minimum transmission were equal to 0.957 and 0.877, respectively. Crystal data for $C_{90}H_{82}B_2Cl_2Co_2P_6 \cdot (2C_6H_6)$, monoclinic space group $P2_1/c$ (#14), a = 26.340(3) Å, b = 13.2151(14) Å, c = 28.015(3) Å, b = 117.909(2)°, V = 8617.6(16) Å^3, Z = 4, D_{calcd} = 1.323 g/cm^3, Abs. Coefficient = 0.607 mm^{-1}, Mo−Kα λ = 0.710 73 Å, T = 98 K, Bruker SMART 1000 CCD, crystal size 0.22 × 0.19 × 0.07 mm^3, θ_{max} = 28.13°, $R1$ = 0.0468, $wR2$ = 0.0660 for $I > 2s(I)$, $R1$ = 0.0995, $wR2$ = 0.0724, G_F ($1/\sigma^2$ weighting) = 1.028, number of reflections collected 106 341 (−34 = h = 33, −16 = k = 17, −37 = l = 36), number of independent reflections 20 585, number of parameters 1027.

X-ray Crystal Structure Analysis of 4. X-ray quality crystals were obtained by vapor diffusion of petroleum ether into a concentrated solution of **4** in benzene. An electric blue crystalline shard was mounted on a glass fiber with Paratone N oil. The structure was solved by direct methods in conjunction with standard difference Fourier techniques. The largest peak and hole in the difference map were 1.060 and −1.086 e.Å^{-3}, respectively. Maximum and minimum transmission were equal to 0.906 and 0.810, respectively. Crystal data for $C_{57}H_{53}BCoIO_2P_3$, monoclinic space group $P2_1/n$ (#14), a = 12.916(3) Å, b = 18.582(4) Å, c = 21.674(5) Å, β = 106.262(3)°, V = 4993.7(18) Å^3, Z = 4, D_{calcd} = 1.409 g/cm^3, Abs. Coefficient = 1.100 mm^{-1}, Mo−Kα λ = 0.71073 Å, T = 98 K, Bruker SMART 1000 CCD, crystal size 0.22 × 0.09 × 0.16 mm^3, θ_{max} = 23.32°, $R1$ = 0.0361, $wR2$ = 0.0602 for $I > 2s(I)$, $R1$ = 0.0547, $wR2$ = 0.0637, G_F ($1/\sigma^2$ weighting) = 1.755, number of reflections collected 54319 (−14 = h = 14, −20 = k = 20, −24 = l = 24), number of independent reflections 7213, number of parameters 586.

X-ray Crystal Structure Analysis of 5. X-ray quality crystals were obtained by vapor diffusion of petroleum ether into a concentrated solution of **5** in benzene. A purple crystal was mounted on a glass fiber with Paratone N oil. The structure was solved by direct methods in conjunction with standard difference Fourier techniques. The largest peak and hole in the difference map were 1.133 and −0.475 e.Å^{-3}, respectively. Maximum and minimum transmission were equal to 0.913 and 0.902, respectively. Crystal data for $C_{53}H_{50}BCoOP_3$, monoclinic space group Cc (#9), a = 17.245(2) Å, b = 16.484(1) Å, c = 16.494(1) Å, β = 109.181(1)°, V = 4428.3(6) Å^3, Z = 4, D_{calcd} = 1.298 g/cm^3, Abs. Coefficient = 0.535 mm^{-1}, Mo−Kα λ = 0.710 73 Å, T = 96 K, Bruker SMART 1000 CCD, crystal size 0.170 × 0.185 × 0.192 mm^3, θ_{max} = 28.61°, $R1$ = 0.0378, $wR2$ = 0.0612 for $I > 2\sigma(I)$, $R1$ = 0.0454, $wR2$ = 0.0624, G_F ($1/\sigma^2$ weighting) = 1.661, number of reflections collected 45 708 (−23 = h = 22, −21 = k = 21, −21 = l = 22), number of independent reflections 10 456, number of parameters 534.

Acknowledgment. We are grateful to the Dreyfus Foundation, the ACS Petroleum Research Fund, and the National Science Foundation (Grant No. CHE-0132216) for financial support of this work. We thank the Beckman Institute (Caltech) for use of the SQUID magnetometer and the crystallographic facility. D.M.J. is grateful for a pre-doctoral fellowship from the National Science Foundation. M.J.A. is grateful for a NDSEG Fellowship. T.A.B. is grateful for a pre-doctoral fellowship from the DOD. J. C. Thomas is acknowledged for assistance with DFT. Finally, we acknowledge our inorganic colleagues at Caltech for many stimulating discussions, and the reviewers of this paper for helpful commentary.

Supporting Information Available: ^{1}H NMR spectra for all complexes; EPR spectrum of **5**; crystallographic data. This material is available free of charge via the Internet at http://pubs.acs.org.

JA026433E